DOE/ET/10815-74
(DE84008052)

Energy

FOSSIL

COLD FLOW MODELING OF PULVERIZED COAL COMBUSTORS FOR MAGNETOHYDRODYNAMIC CHANNEL APPLICATIONS

Topical Report

By
R. J. Schulz
T. V. Giel
A. Ghosh
R. D. Morris

March 1984

Work Performed Under Contract AC02-79ET10815

The University of Tennessee Space Institute
Energy Conversion Research and Development Programs
Tullahoma, Tennessee

Technical Information Center
Office of Scientific and Technical Information
United States Department of Energy

DISCLAIMER

DISCLAIMER

This report has been reproduced directly from the best available copy.

Available from the National Technical Information Service, U. S. Department of Commerce, Springfield, Virginia 22161.

Price: Printed Copy A04
Microfiche A01

Codes are used for pricing all publications. The code is determined by the number of pages in the publication. Information pertaining to the pricing codes can be found in the current issues of the following publications, which are generally available in most libraries: *Energy Research Abstracts (ERA); Government Reports Announcements* and Index (*GRA* and I); *Scientific and Technical Abstract Reports (STAR);* and publication NTIS-PR-360 available from NTIS at the above address.

DOE/ET/10815--74
DIST. CATEGORY UC-90g
(Special)
[TR-4.3.6-82-01]
UTSI-82-18

DOE/ET/10815--74

DE84 008052

COLD FLOW MODELING OF PULVERIZED COAL COMBUSTORS FOR MAGNETOHYDRODYNAMIC CHANNEL APPLICATIONS

TOPICAL REPORT

Prepared by:

R. J. Schulz
T. V. Giel
A. Ghosh
R. D. Morris

The University of Tennessee Space Institute
Energy Conversion Research and Development Programs
Tullahoma, Tennessee 37388

PREPARED FOR THE UNITED STATES
DEPARTMENT OF ENERGY

March 1984

Under Contract No. DE-AC02-79ET10815

DOE/ET/10815-74
(UTSI-82-18)
(DE84008052)
Distribution Categories UC-90g and UC-93

COLD FLOW MODELING OF PULVERIZED COAL COMBUSTORS FOR MAGNETOHYDRODYNAMIC CHANNEL APPLICATIONS

TOPICAL REPORT

Prepared by:

R. J. Schulz
T. V. Giel
A. Ghosh
R. D. Morris

The University of Tennessee Space Institute
Energy Conversion Research and Development Programs
Tullahoma, Tennessee 37388

PREPARED FOR THE UNITED STATES
DEPARTMENT OF ENERGY

March 1984

Under Contract No. DE-AC02-79ET10815

ABSTRACT

This report describes an experimental program and techniques for studying the internal aerodynamics of pulverized coal combustors of the type used in magnetohydrodynamic test trains at The University of Tennessee Space Institute. The combustors are modeled with small scale, cold flow models that permit both flow visualization and velocity field surveys to be performed. Water was selected as the working fluid so that the model flow fields had the same Reynolds number as the actual reactive combustors, and also to facilitate flow visualization. The systems used for flow visualization and velocity field surveying are described in detail. The velocity field survey equipment is based on a vector-velocity, laser doppler velocimeter coupled to a controllable field scanning device and a microprocessor for on-line data reduction. Results are presented that were obtained from a laser velocimeter study of recirculating flows in a combustor model. The results show that, even for exceedingly simple geometrical arrangements of oxidant injector configurations, complex three dimensional highly turbulent flow fields exist in the combustor. A brief discussion of the impact of the results on fuel injector positioning is presented.

CONTENTS

FIGURES

APPENDIX FIGURES

NOMENCLATURE

C	Concentration
f	Frequency
f_c	Clock Frequency
I	Photomultiplier Tube Current
I_{max}	Maximum Signal Amplitude
I_{min}	Minimum Signal Amplitude
k	Turbulence Kinetic Energy
K_H	High Count
K_L	Low Count
n	A Number
N	A Number of Signal Pulses
N_S	Short Count Signal Pulses
N_L	Long Count Signal Pulses
n_S	Short Clock Count
n_L	Long Clock Count
p	Fluid Pressure
T	Fluid Temperature
t	Time
u	x Component of Velocity
v	y Component of Velocity
V	Visibility
w	z Component of Velocity
x	Coordinate of Cartesian Coordinate System
y	Coordinate of Cartesian Coordinate System
z	Coordinate of Cartesian Coordinate System

Overbar

$\overline{\quad}$ Time Averaged

Superscript

$'$ Fluctuation in Variable

Greek Symbols

δ Fringe Spacing

ϵ Aperiodicity

ρ Fluid Density

1.0 INTRODUCTION

1.1 Background

The Energy Conversion Research and Development Programs (ECP) of The University of Tennessee Space Institute (UTSI) is conducting research, development and testing of a pilot scale system that could serve as a system for testing power generators for cycle augmentation of coal fired, steam generating power plants. The current research is directed toward the evaluation of the heat recovery, seed recovery and pollutant control characteristics of a radiant furnace and secondary combustor system. The open cycle test train at the Coal Fired Flow Facility (CFFF) is shown schematically in Figure 1. The flow processes that occur in this cycle begin with coal, which is pulverized together with a seed material (e.g. K_2CO_3) and fed to a combustor where it is injected, mixed with vitiation-heated oxidizer and burned, producing high temperature gas that is electrically conducting. The gas, which in the UTSI design contains all of the slag species in vapor or liquid form, flows out of the combustor through a transonic nozzle and into a magnetohydrodynamic channel contained between the poles of a magnet. The gas flow leaves the channel after doing work against the magnetic field and enters a flow decelerator or diffuser. Downstream equipment removes heat and slag from the flow to generate steam for conventional power producing cycles.

One objective of the research conducted by the ECP is to optimize the vitiation heater, the coal combustor, and the nozzle components of this flow system to provide the channel with electrically conducting gas of uniform velocity, temperature and conductivity to (i) optimize power extractions, and (ii) insure reliability of the components while minimizing heat loss, corrosion and component performance degradation. To define the research, it is necessary to describe the details of the combustor system. Figure 2 is a schematic of the primary combustor configuration.

Since the UTSI combustor is based on passing 100 percent of the combustion-generated slag through the nozzle, channel and diffuser, the combustor configuration design is based on the aerodynamics of multiple, parallel, turbulent jets aligned with the axis of the combustor. The jets are created by multiple, round, parallel holes passing through a plate, normal to the combustor axis, called an injector or disperser plate, shown schematically in Figure 2 and in detail in Figure 3. The plate creates a two-stage combustion process by dividing the combustor volume into an upstream vitiation heater with a small fuel flow and a downstream coal combustor where the main fuel mass is burned. The gas from the vitiation heater passes through the disperser plate holes creating jets of hot (typically about 1111K) oxidizer. The oxidizer jets mix with the fuel, pulverized coal and/or fuel oil, which is injected through nozzles. The coal nozzle is a centrally located, plugged pintle variety. The primary combustor design variables are the oxidizer hole diameters, the number of holes, the radii of the concentric rings of these holes from the centerline of the combustor, and the characteristics of the fuel oil and pulverized coal injection nozzles. Figure 4 schematically illustrates the type of flow created by the disperser plate. Research is underway at UTSI to investigate the effects of variations of these fundamental parameters on the combustor performance, internal aerodynamics, slagging characteristics, and heat flux distributions on the walls.

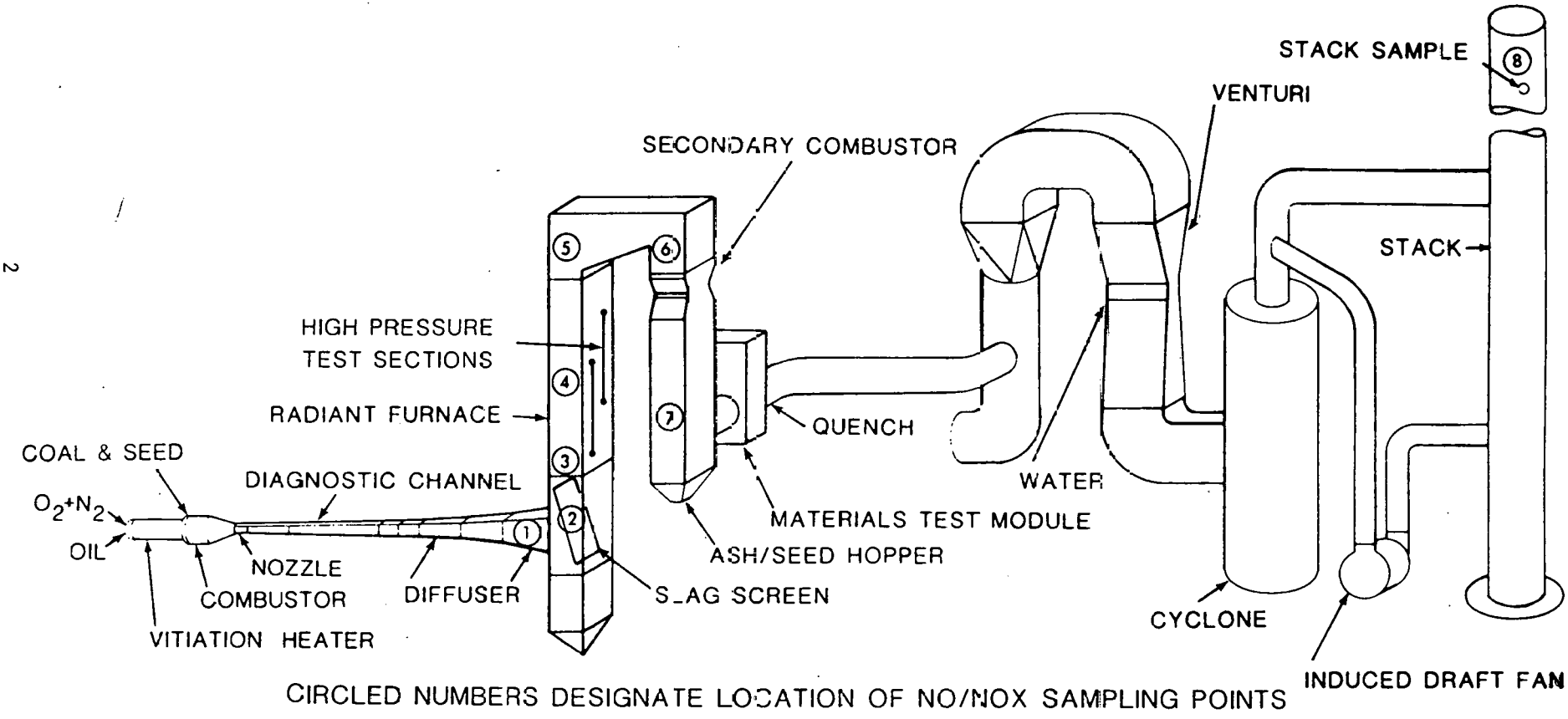

LMF-1 TEST TRAIN CONFIGURATION

Figure 1. Schematic of CFFF Power Train

a. Porous Plate Flow Straightner
b. Fuel Oil Line & Central Support Sting
c. Spark Igniter
d. Porous Plate for Mixing & Injection of Fuel Oil
e. Oil Injectors
f. Coal Tube
g. Cast Refractory
h. Disperser Plate
i. Oil Injectors
j. Coal Tube Vaned Plug
k. Refractory Lining

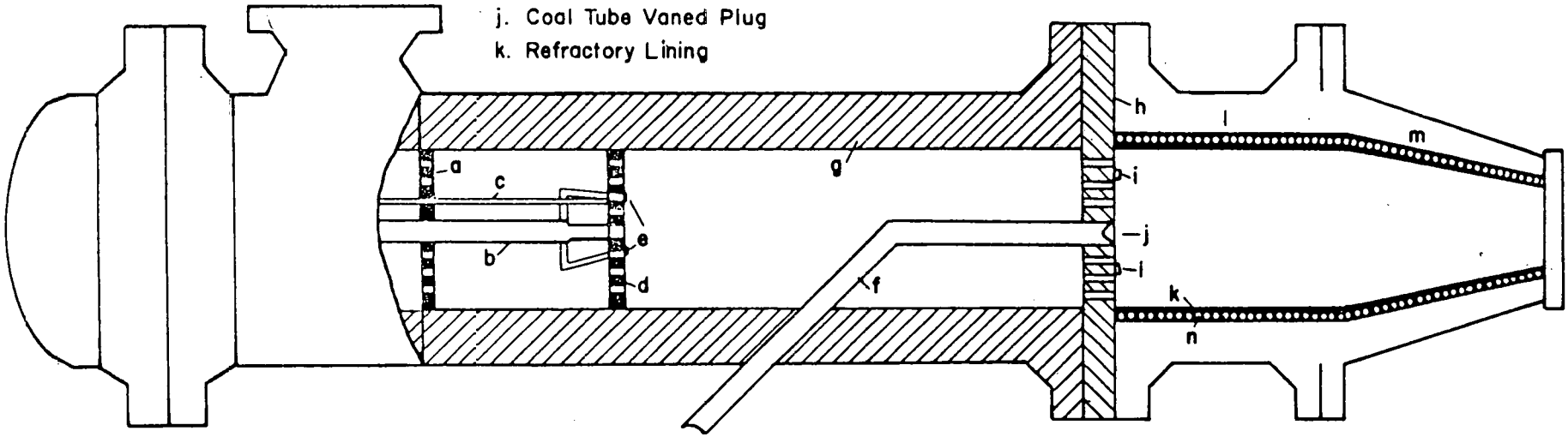

l. Cylindrical Section
m. Conical Section
n. Cooling Tubes

Figure 2. Schematic of Vitiation Heater and Primary Combustor Hardware

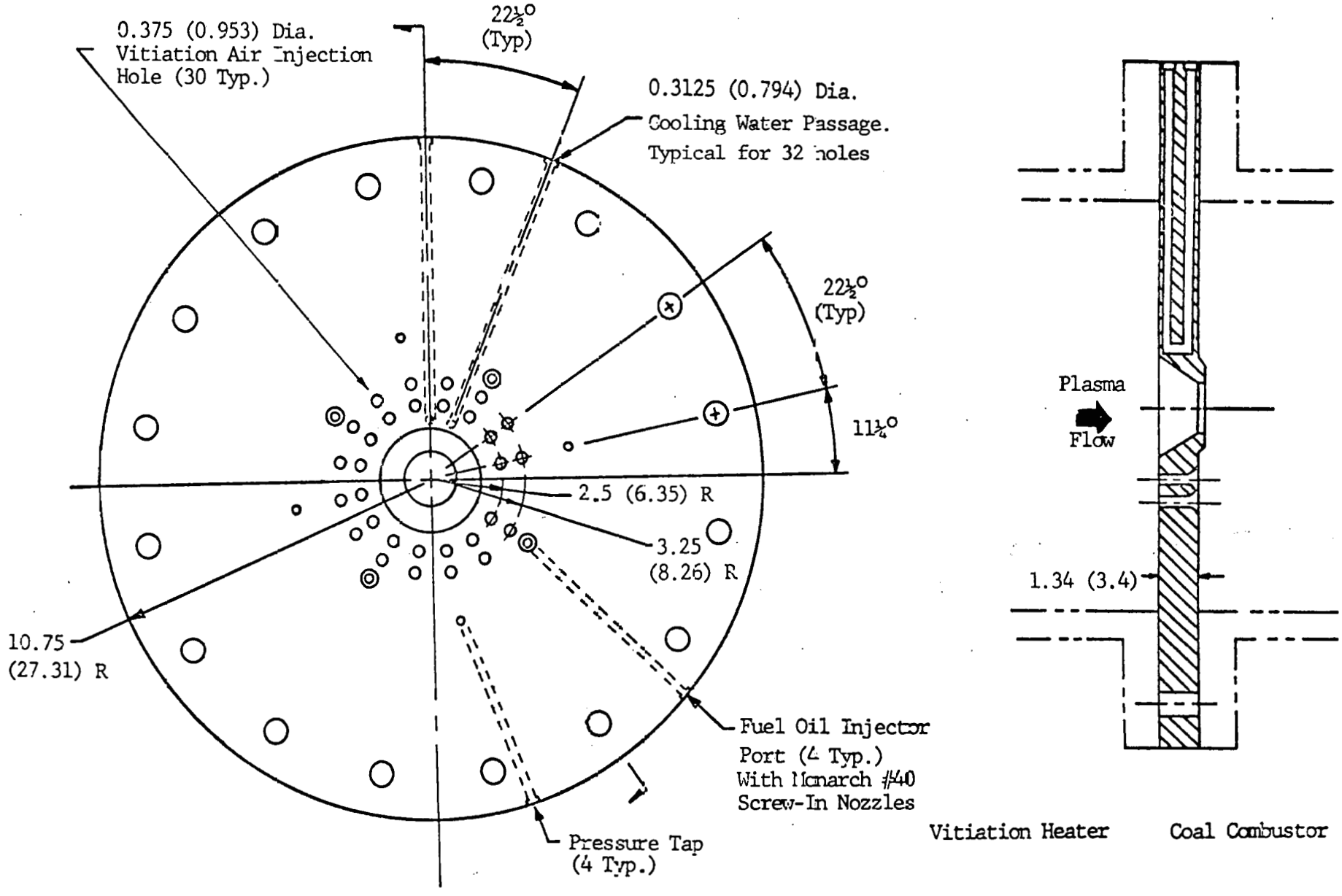

Note: Dimensions in inches (cm)

Figure 3. Schematic Drawing of Typical Disperser Plate

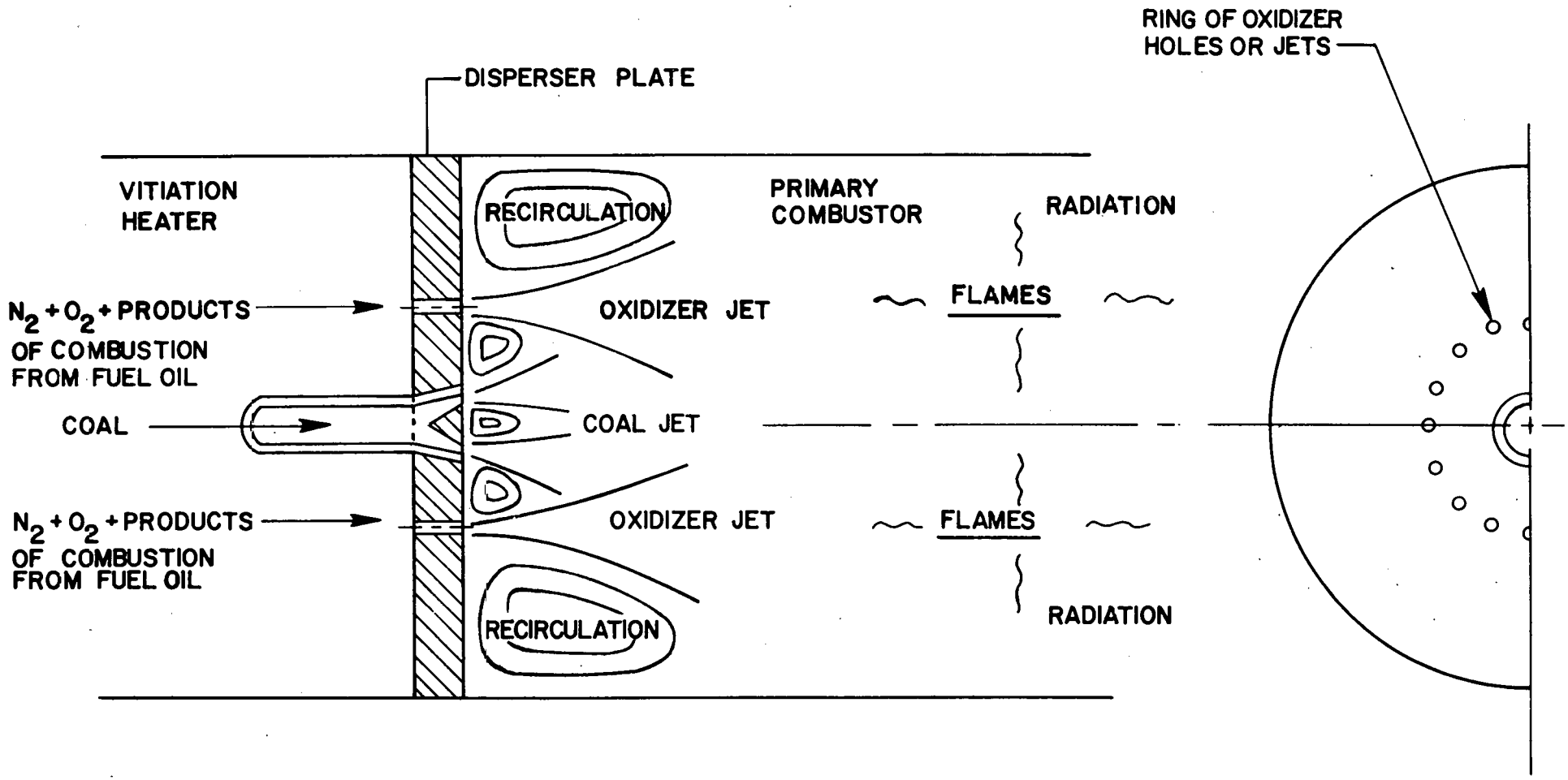

Figure 4. Simplified Schematic of Primary Combustor Flow Field Created by Disperser Plate

To minimize heat loss, the combustor surface area is minimized so that the space heat release rate is of the order of 1.4903×10^8 J/m^3/sec. Compact combustors have been developed for industrial use that operate based on either swirling or recirculating flows or both. The UTSI combustor does not provide swirl but does depend on aerodynamically generated and controlled recirculation through the mechanisms of jet mixing and entrainment. The jets are designed to:

1) Entrain and mix thoroughly the pulverized coal (and seed material) with the oxidizer in a compact cylindrical combustor;

2) Establish sufficient fuel residence times in the combustor to provide for coal particle pyrolysis, fixed carbon and volatiles utilization and combustion, and permit slag species vaporization;

3) Decay quickly and efficiently so that the characteristic jet-like velocity, temperature and species profiles (which are Gaussian or cosine profile shaped) become uniform or flat, thus providing homogenous, high temperature, uniform electrical conductivity flow at the nozzle inlet plane, without inducing flame impingement on the combustor or nozzle walls; and

4) Provide a sufficiently high bulk gas velocity to promote slag rejection at a 100 percent rate from the combustor volume so that it passes out through the generator.

The key parameters controlling the combustor aerodynamics and combustion kinetics are: (i) composition of the coal, (ii) coal particle size distributions, (iii) temperature and composition of the vitiation gas, (iv) number and diameter of the oxidizer holes in the disperser plate, (v) geometrical placement of oxidizer holes over the surface of the plate, and (vi) design and operation of the coal injection nozzle which is located on the combustor centerline and the fuel oil nozzles at the periphery. Note also that the coal is seeded to about 10% by weight with potassium carbonate before being pulverized, piped and injected into the combustor. The combustor flow field is controlled mainly by the gas jets from the oxidizer holes and the carrier gas flow provided in the coal stream. The UTSI combustor is based on very dense phase coal flow, with negligible carrier gas, where the coal particles become distributed in the combustor as a result of:

1) Particle size and injection velocity,

2) Aerodynamic drag acting on the coal particles caused by a flow field essentially created by oxidizer jet mixing and interaction, and

3) Turbulent fluctuations or effective turbulent diffusivity created by the turbulence from the interacting gas jets (which can have an extremely large effect).

For other systems, where coal flow is injected into a combustor with appreciable amounts of secondary carrier gas, the combustor aerodynamic flow can be significantly affected by the gas injected with the coal because this gas "satisfies the entrainment capacity" of the oxidizer jets and therefore significantly affects the rates of jet spreading and decay.

The effect of added secondary gas flow on ducted jet mixing and recirculation has been observed experimentally, for example, references 1-3. In this case, the coal would become distributed in the combustor not only by the causes identified above, but also by the interactive aerodynamics of the coal carrier gas jet with the multiple surrounding oxidizer jets. The present UTSI coal/seed supply and injection system is based on negligible carrier gas in the feed system, so that the oxidizer jets are primarily responsible for the combustor aerodynamics.

1.2 Research Required

The research required to permit the development of mathematical models of combustor flows consists of two parallel efforts. The primary effort is to conduct experimental investigations of combustor flows to generate data for comparison to the predictions and for basic understanding of the physics of the processes in the combustor. The second effort is to develop efficient and accurate numerical solution procedures for solving the mathematical system of governing equations. This includes the evaluation and development of turbulence transport models for heat, mass and momentum, in itself a formidable task.

The data needed from an experimental combustor research program include the following:

1) Time-mean flow field variables: $\overline{u}$, $\overline{v}$, $\overline{w}$, $\overline{p}$, $\overline{T}$, $\overline{\rho}$ and $\overline{C}$

2) Fluctuating flow field quantities that define turbulence structure and turbulence transport of heat, mass and momentum: $\overline{u'^2}$, $\overline{v'^2}$, $\overline{w'^2}$, $k = 1/2\ (\overline{u'^2} + \overline{v'^2} + \overline{w'^2})$, $\overline{\rho u'v'}$, $\overline{u'T'}$, $\overline{v'T'}$, $\overline{w'T'}$, $\overline{\rho'T'}$, $\overline{\rho'C'}$, $\overline{p'u'}$, $\overline{p'u'v'}$, and others. The theoretical number of these turbulent correlation functions in reactive turbulent flow is enormous as shown by Bray, reference 4. Hopefully, not all of these correlations are required to develop useful turbulent transport models for reactive flows. Current transport models are limited to modeling relatively few of the correlations because data defining the importance or the physical meaning of most of the correlations are not yet available in the literature.

3) Data defining the location and extent of the recirculation zones, shear layer reattachment points, and, whether the flow in the combustor is steady or unsteady.

The data are required for both isothermal and reactive flows in combustors. For reactive combustors, the flows are relatively more complex than in isothermal environments. In particular, in the UTSI pulverized coal combustor, the combustion chemistry is based on flames of particulates, the pulverized coal, seed and atomized oil droplets. The coal spray is formed by a nozzle-ejected cloud containing specific size-class coal and seed particles. In the current system, the seed and coal are pulverized together to a powder with a mass mean diameter of about 45 microns. The physical mechanisms of coal particle pyrolysis are coupled to

the combustor aerodynamics and the fundamental mechanisms that govern the chemical destruction of "coal" and oxidizer and the formation of gaseous products of combustion, including the vaporized slag species. The high temperatures within the combustor also produce significant thermal radiation which in turn affects the heat flux to the coal particles and therefore the rates of particle combustion. The coupling of all these processes may be indicated schematically as shown by the arrows below.

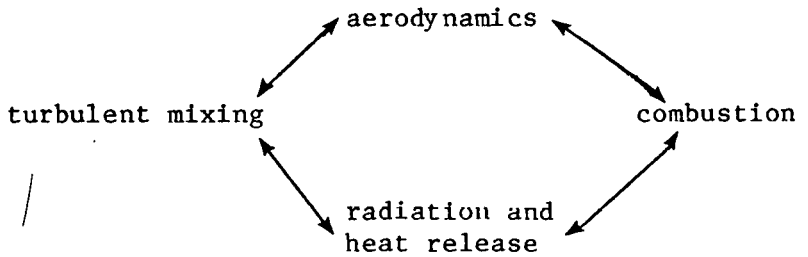

The mechanisms of the coupling are presumed to be described by the correlations indicated, but the correlations, being numerous and not yet physically modeled, must either be determined by experiment, empirically modeled, or neglected.

Because the physical processes in the combustor are so complex, and details of the flow are difficult to assess, many simplifications are required in the experimental investigation. One major simplification is to study cold, isothermal flows where detailed surveys of the internal aerodynamics can be obtained with relative ease and efficiency. Additionally, it has been found that the cold flows possess the essential qualitative features of the hot or reactive flows (e.g. recirculation zone structure, nondimensionalized pressure distributions, velocity distributions, and basic stability or instability behavior) while differing in certain quantitative areas, for example, such as the lengths or extents of the recirculation zones, the rates of decay of maximum velocity, and the point-wise turbulence structure. Experience has shown, however, overwhelming benefits from performing cold flow experiments, to obtain information on such flows which permits the reactive flows to be qualitatively understood and permits the verification or calibration of mathematical models of the combustor flows. Thus, a critical need exists for isothermal test data from combustor models for the purposes described.

1.3 Research In Progress

The cold flow research in progress consists of fabricating plexiglas combustor configurations and evaluating them in a water tunnel flow circuit. The primary component being modeled is the disperser plate.

Two types of data acquisition are employed, namely, flow visualization and laser doppler velocimetry. Flow visualization provides a qualitative understanding of the nature of the combustor flow fields, including

steadiness or instability modes. The flow is made visible by injecting air and hydrogen gas bubbles, and also various dye materials into the flow. In-situ or photographic observations of the bubble motions and patterns provides the basic flow visualization. The laser doppler velocimeter is a device for obtaining direct, quantitative data on the internal flow field variables. The technique is non-intrusive, no mechanical probing of the flow is required. The device, described in detail in Section 3 and Appendix A, measures two instantaneous velocity components in the flow. The electronic circuitry developed for use with this instrumentation analyzes the velocity components being measured and converts them into time averaged or mean values, and also their statistically averaged fluctuation quantities, that is, into $\overline{u}$ and $\overline{v}$, and $\overline{u'^2}$, $\overline{v'^2}$ and $\overline{u'v'}$, respectively. The laser velocimeter provides direct measurements of both the time averaged flow in the combustor and the structure of the turbulence within the combustor. The data can be interpreted to establish the expected rates of diffusion of heat, mass and momentum in the recirculating combustor flows.

The data described above are used to optimize disperser plate technology by evaluation of many different disperser plate configurations. Each configuration is characterized by a relatively unique hole pattern consisting of hole sizes and their number and distribution over the face of the plate. The optimum plate design will be one that: 1) provides a steady turbulent flow in the combustor with acceptable pressure fluctuation levels, 2) produces the most uniform velocity and turbulent intensity profiles at the combustor outlet station, 3) establishes recirculation zones of acceptable size with turbulence levels high enough for intense mixing of fuel and oxidizer, and 4) has an acceptable pressure loss level.

1.4 Research Planned

A series of tests is in progress for a variety of disperser plate designs that have different injector hole patterns and hole sizes. The disperser plate designs will be for both single and multiple coal injector configurations, hence, disperser plates with clusters of geometrically similar oxidant injector hole patterns will be tested. The fundamental aerodynamic environment created by each of these configurations will be mapped in detail, together with the flow visualization studies. Designs for actual disperser plate geometries will be developed for testing in the existing coal fired flow trains at UTSI.

2.0 DESCRIPTION OF TEST APPARATUS

2.1 Test Site and Shelter

A site for the cold flow test circuit installation was selected that provides both water and air supplies of adequate size.

Figure 5 is a photograph of the exterior of the shelter, which also shows the concrete pad extending past the shelter. The concrete pad was designed to support water tanks that are reservoirs for the water tunnels.

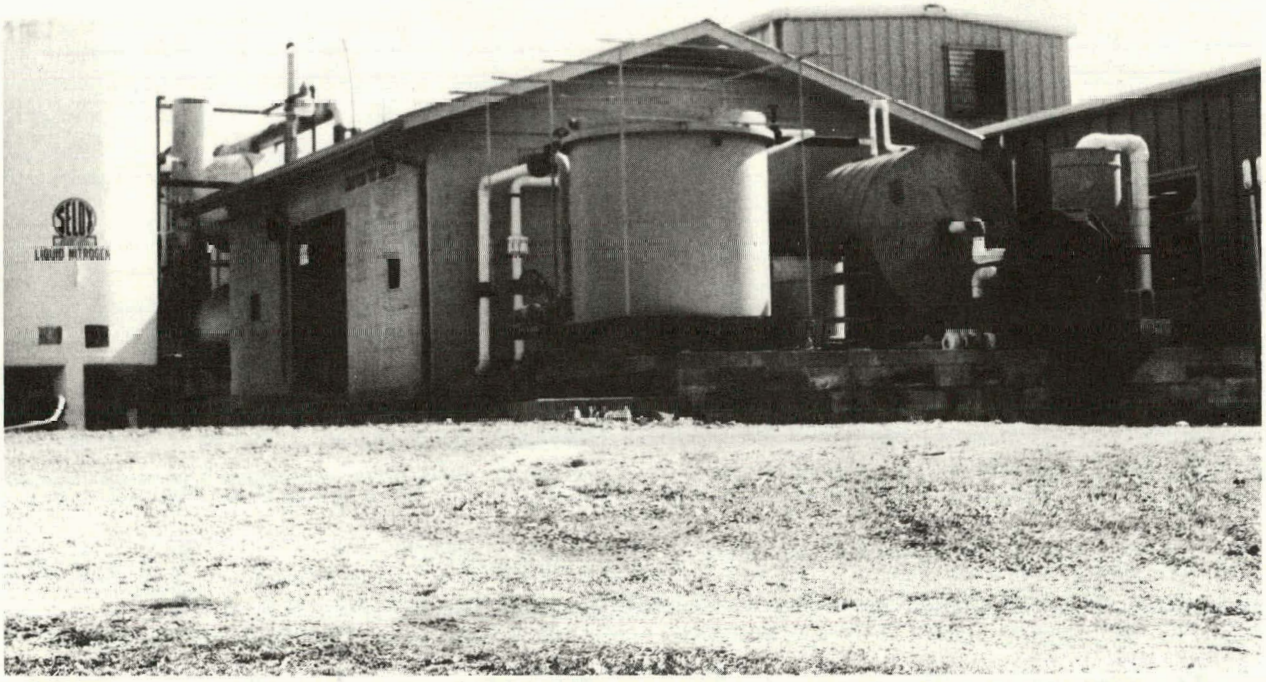

Figure 5. Photo of Test Shelter

Because a laser-based flow field survey system is used in the shelter, a pair of rotating warning beacons is installed on the outside of the shelter to alert workers outside the building to not enter while the laser is in operation. Of course, workers inside the building are protected by the appropriate safety goggles and other equipment during laser operation. A laser beam stop is connected electrically to the shelter door. Anyone from outside who opens the door automatically triggers the beam to stop. This is another safety precaution.

2.2 Water Tunnel Flow Circuit

Currently three flow circuits are installed in the test shelter. One is an air tunnel in which a diffuser model is installed, Figure 6. The other two flow circuits are water tunnels, one of which is shown in Figure 7. A plexiglas model of the primary combustor is installed in this water flow circuit. The model consists of a disperser plate, a cylindrical combustor section, and a contracting outlet section. The remainder of the flow circuit is made up of a water tank, both Plexiglas and PVC ducting, water pumps and water filters. A schematic of the flow circuit is shown in Figure 8.

Water is continuously circulating through the tank and main piping system during testing. At the same time, water is continuously being withdrawn from the tank, filtered, and re-added to the tank by an auxiliary pump, piping and filter system.

2.3 Model Combustors

The model combustor is shown schematically in Figure 9. The principal components of the combustor are shown in Figures 10-12. A disperser plate currently installed in the system is shown schematically in Figure 10 and photographically in Figure 11. The dimensions of the system are shown in Figure 12.

The disperser plate can be axially traversed along the Plexiglas duct to axially shift the entire flow field created by the disperser plate relative to a fixed window position. By this technique radial flow field surveys can be obtained at any desired distance downstream of the plate. When the disperser plate is moved, the conical outlet or contracting section is also moved to keep the axial distance between these components fixed.

A 0.95 cm wide slot was cut into the wall of the combustor cylindrical section to provide undistorted optical access for the laser beam. The slot is surrounded by a windowbox arrangement, Figure 12, which also contains water. The windowbox serves to provide a deep cavity surrounding the slot cut into the combustor wall. The deep cavity reduces the perturbations that might be created in the combustor flow by the slot. The slot and window cavity configuration was designed after an arrangement used previously in a highly successful combustor research program that also used that same laser velocimeter techniques, Reference 3.

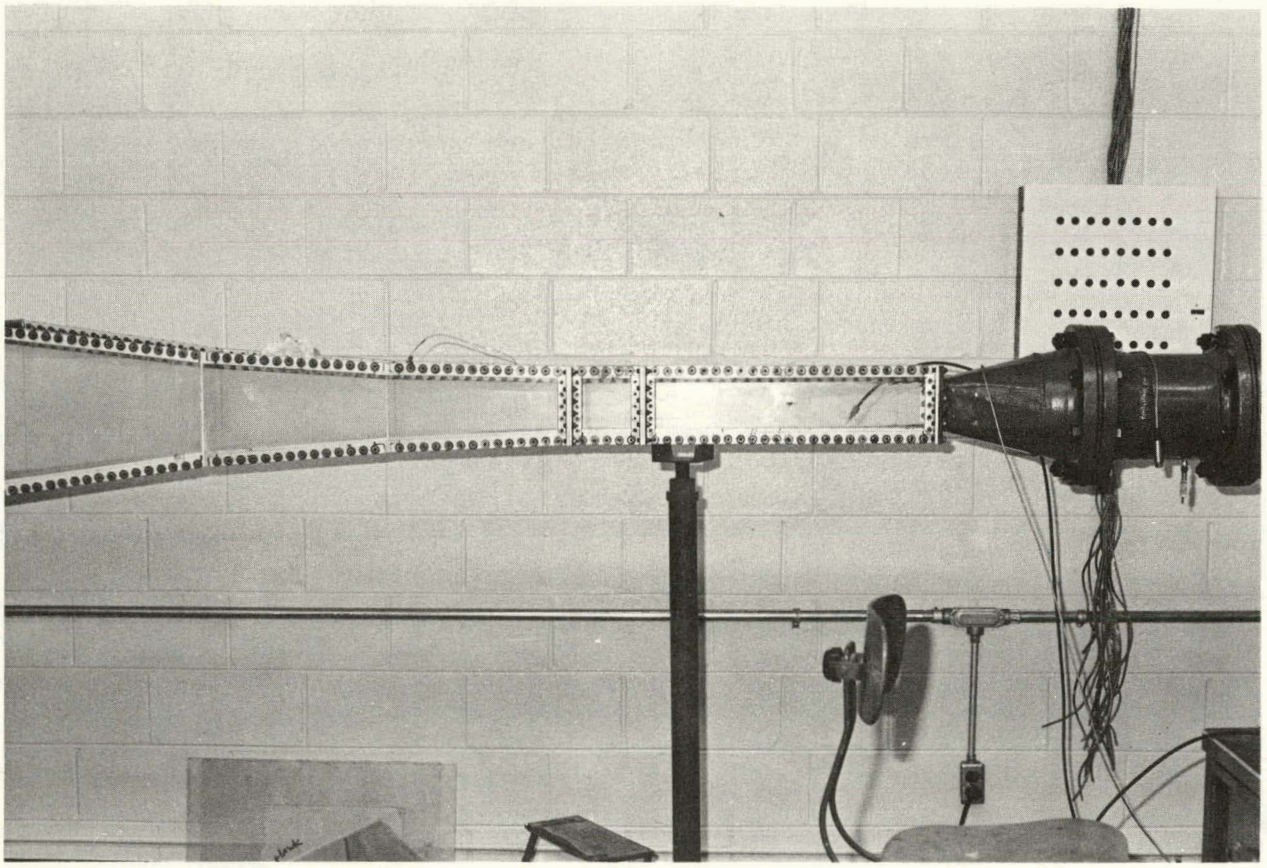

Figure 6. Photo of Diffuser Model Installed in Air Tunnel

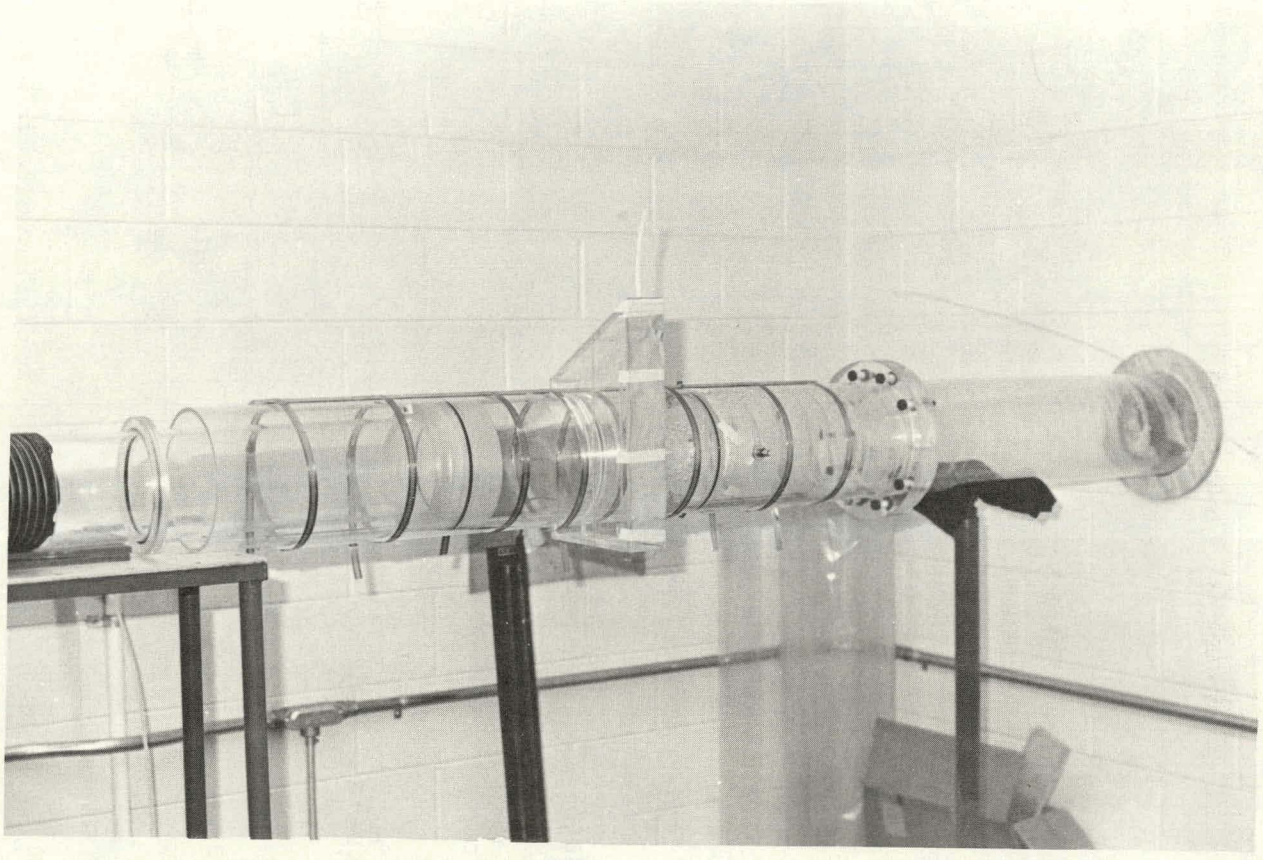

Figure 7. Photo of Combustor Model Installed in Water Tunnel

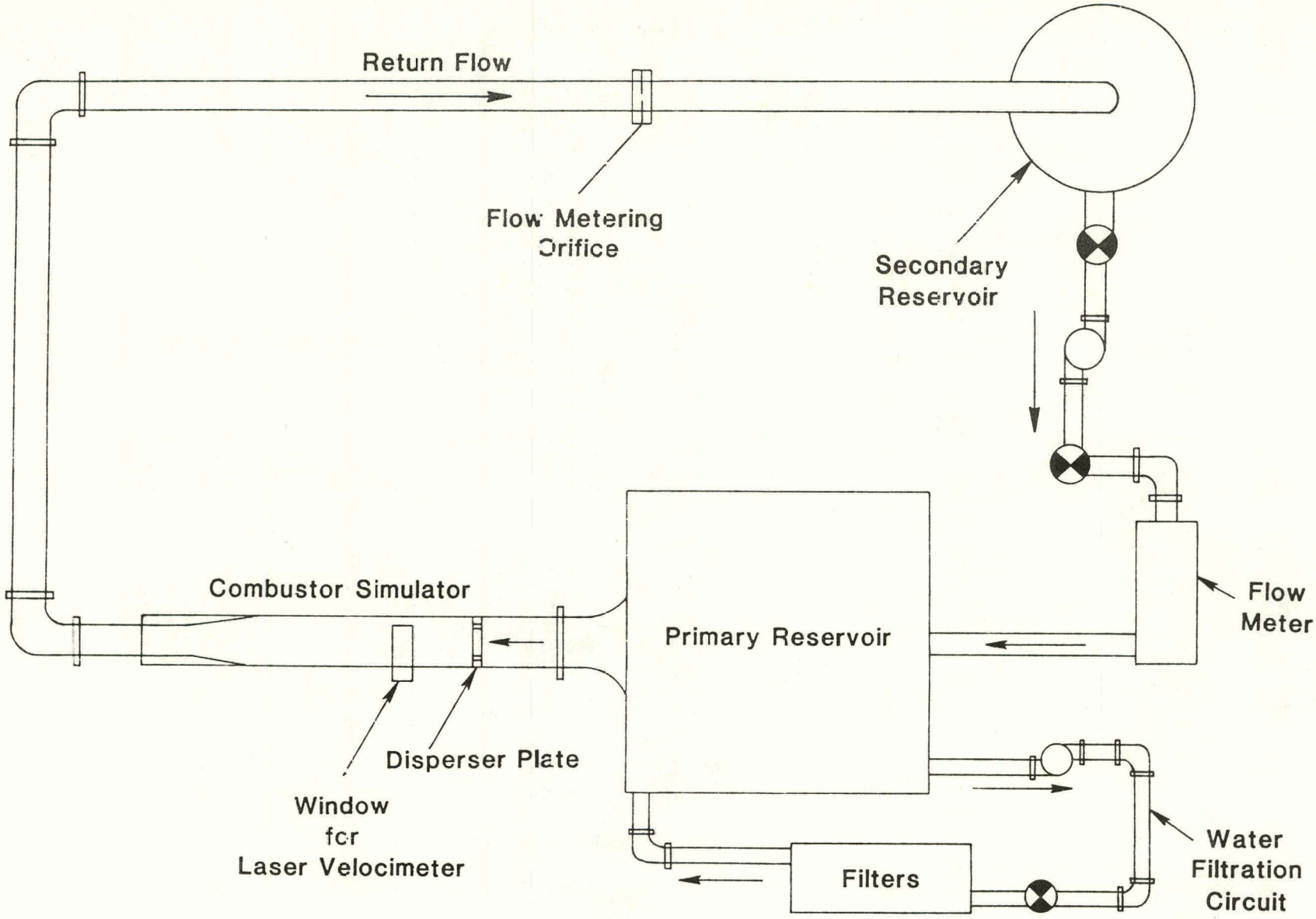

Figure 8. Schematic of Water Tunnel Flow Circuit

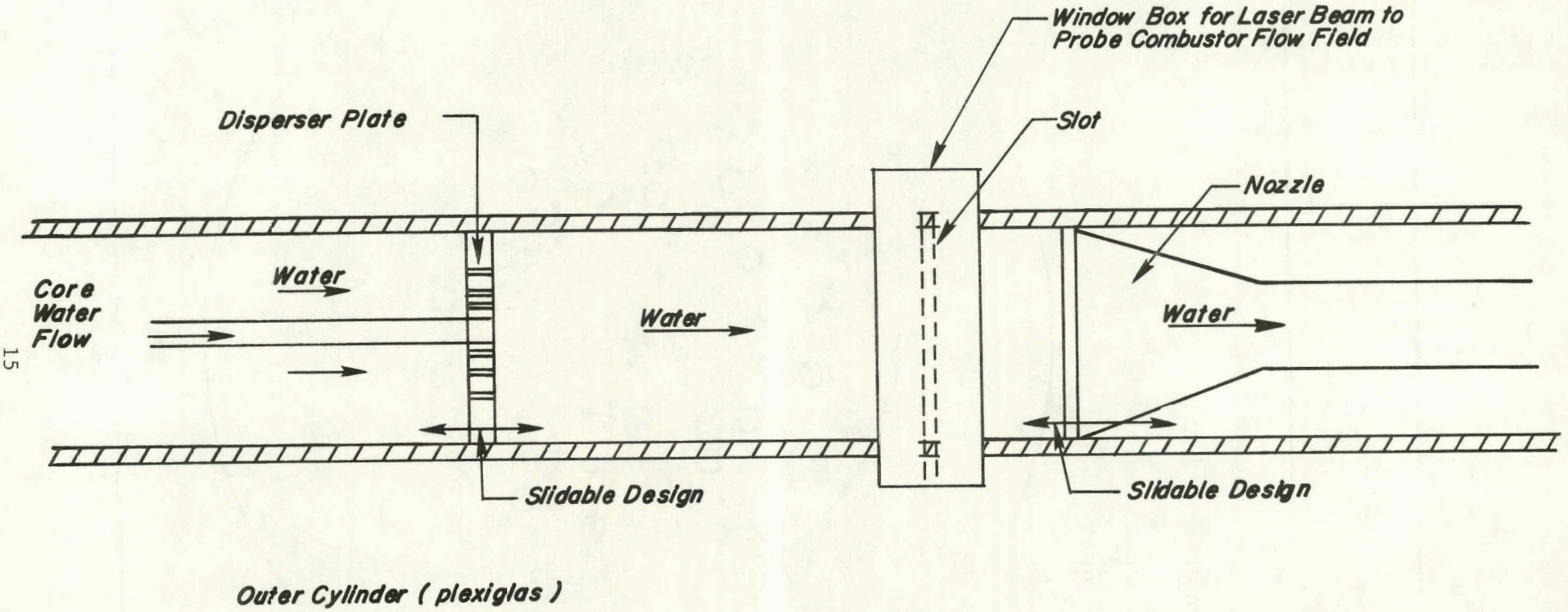

Figure 9. Schematic of Combustor Model Installed in Water Tunnel

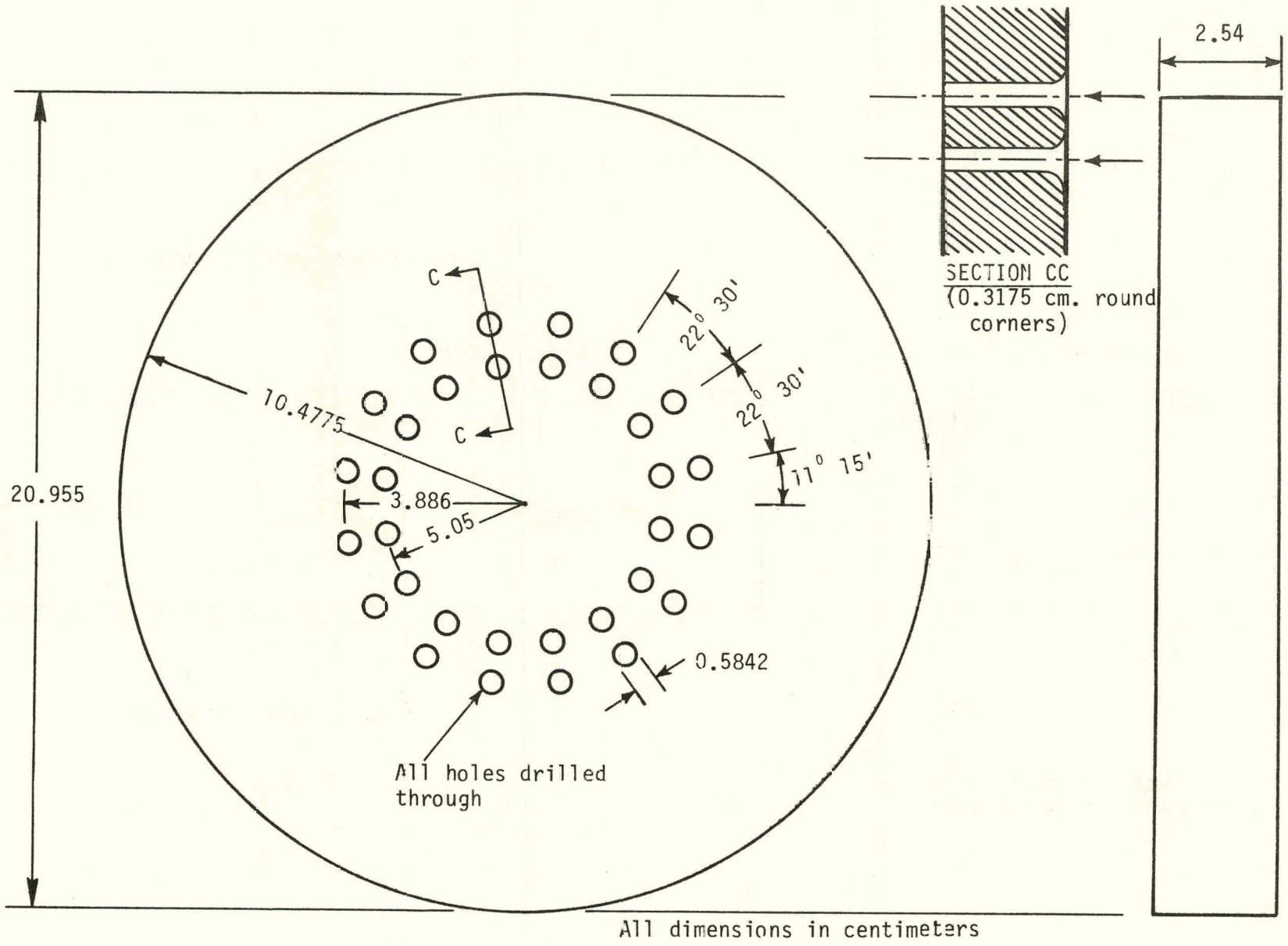

Figure 10. Schematic of Disperser Plate Model

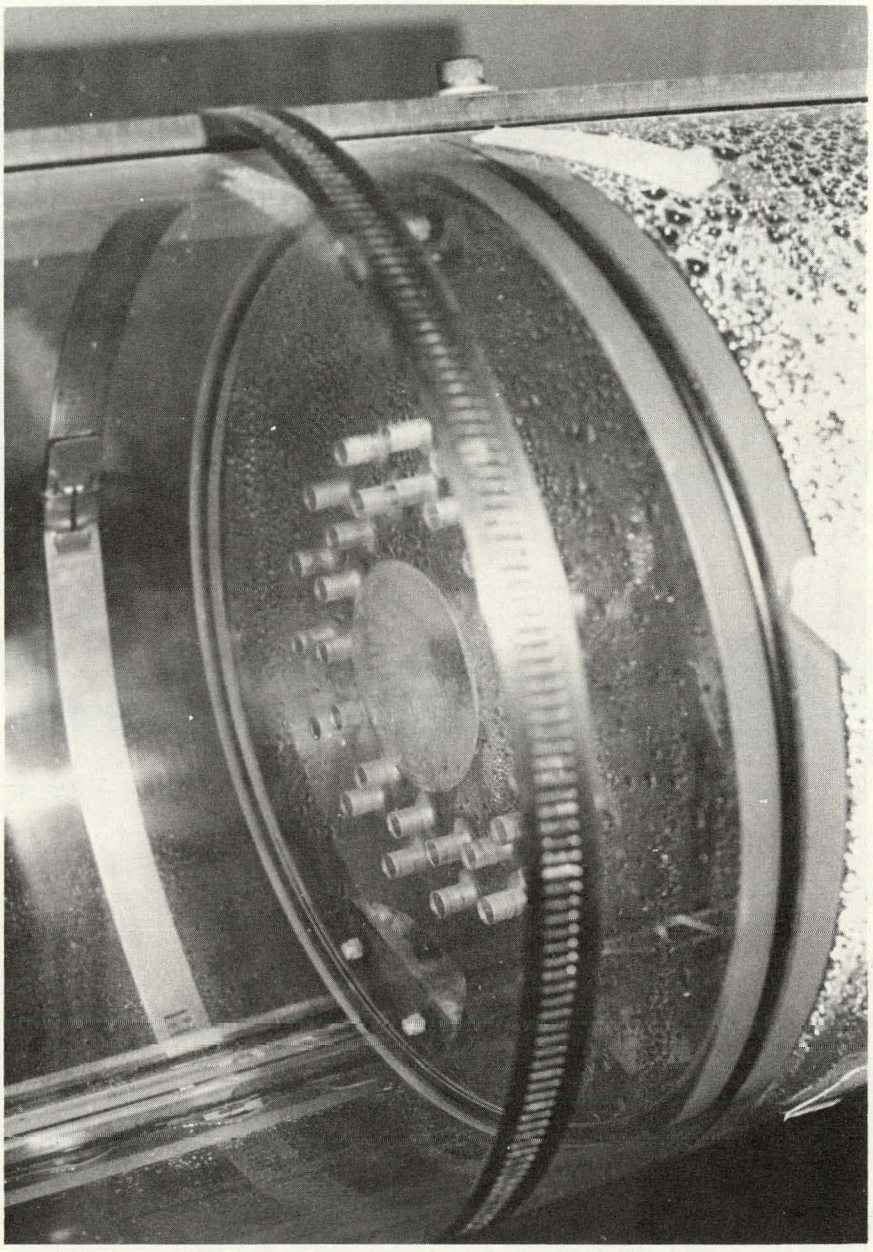

Figure 11. Photo of Disperser Plate Installed in Combustor Model

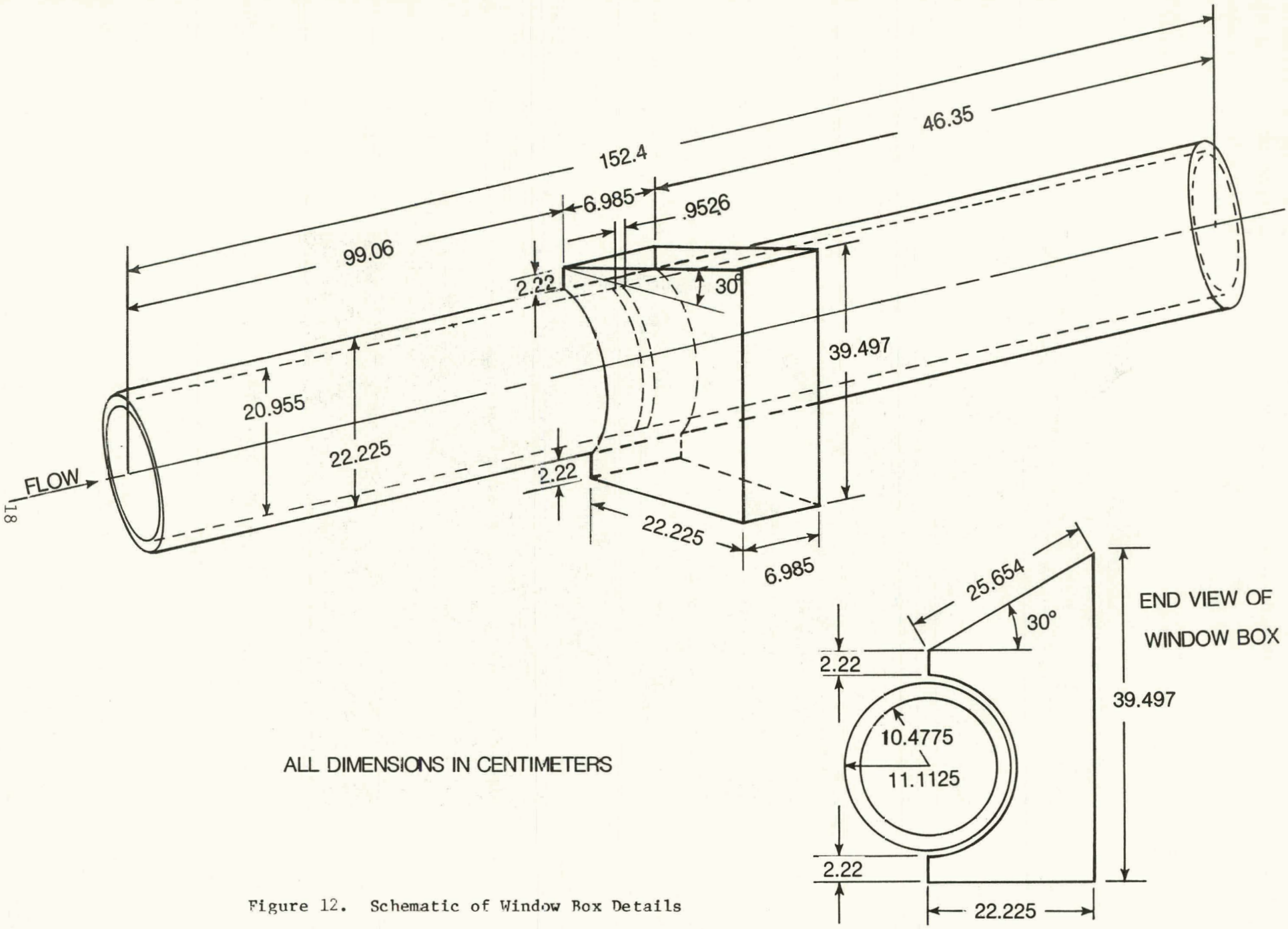

ALL DIMENSIONS IN CENTIMETERS

Figure 12. Schematic of Window Box Details

3.0 DATA ACQUISITION SYSTEM

3.1 Laser Vector Velocimeter

3.1.1 Introduction

The Laser Vector Velocimeter (LV), is designed to simultaneously measure two orthogonal vector components of velocity in a particle laden flow. The instrument divides into three basic subsystems: (i) the optical system (ii) the signal processing system and (iii) the data acquisition system.

3.1.2 Optical System

A schematic of the Laser Vector Velocimeter (LV) optical system is shown in Figure 13. It utilizes a four watt Argon ion laser manufactured by Lexel. The laser is mounted on a 60.96 cm x 121.92 cm thick aluminum base plate which also holds the transmitting and receiving optical systems. A water-filled ultrasonic Bragg cell with x-cut 5 MHz fundamental frequency quartz transducer crystals operating at 15 and 45 MHz overtones is used to beam split and frequency shift the input laser beam into four beams having a common center. The frequency shifts are used to determine velocity directions and identify components. The Bragg cell crystals are driven by a power amplifier which is referenced to a local oscillator circuit common to both the signal separator electronics and the power amplifier. In this way, errors because of differences in frequency between the Bragg cell and signal separator mixers are eliminated. Lenses are used to focus the beams to the measurement position, called the probe volume. The lens train is mounted on optics rails to position the probe volume where desired. A zoom lens system is also used to vary probe volume diameter and fringe period. The present optical system was designed to be used in a backscatter observation mode and the backscatter collection optics were mounted in a vertical plane immediately above the transmitting lenses. In this configuration, the receiving optical system can be focused on any probe volume position. For example, when the probe volume is focused 50.8 cm in front of the output of the transmitting optics, the receiving optics subtend an angle of approximately 20°. This provides for high spatial resolution for the scattered light receiver giving a depth of field of about six probe volume diameters. The backscatter receiving lens is an F/2.4 projection lens which is capable of collecting a large solid angle of scattered light. It should be noted that the design is such that forward scatter observation can be obtained by decoupling the receiver from the transmitter. The photodetector is an EMI 9781R photomultiplier tube with approximately 12% quantum efficiency for the major wavelengths of the Argon ion laser. Figure 14 is a photograph of the assembled optical system. The entire base plate is mounted on a mill bed which has been modified to produce three motorized scan directions.

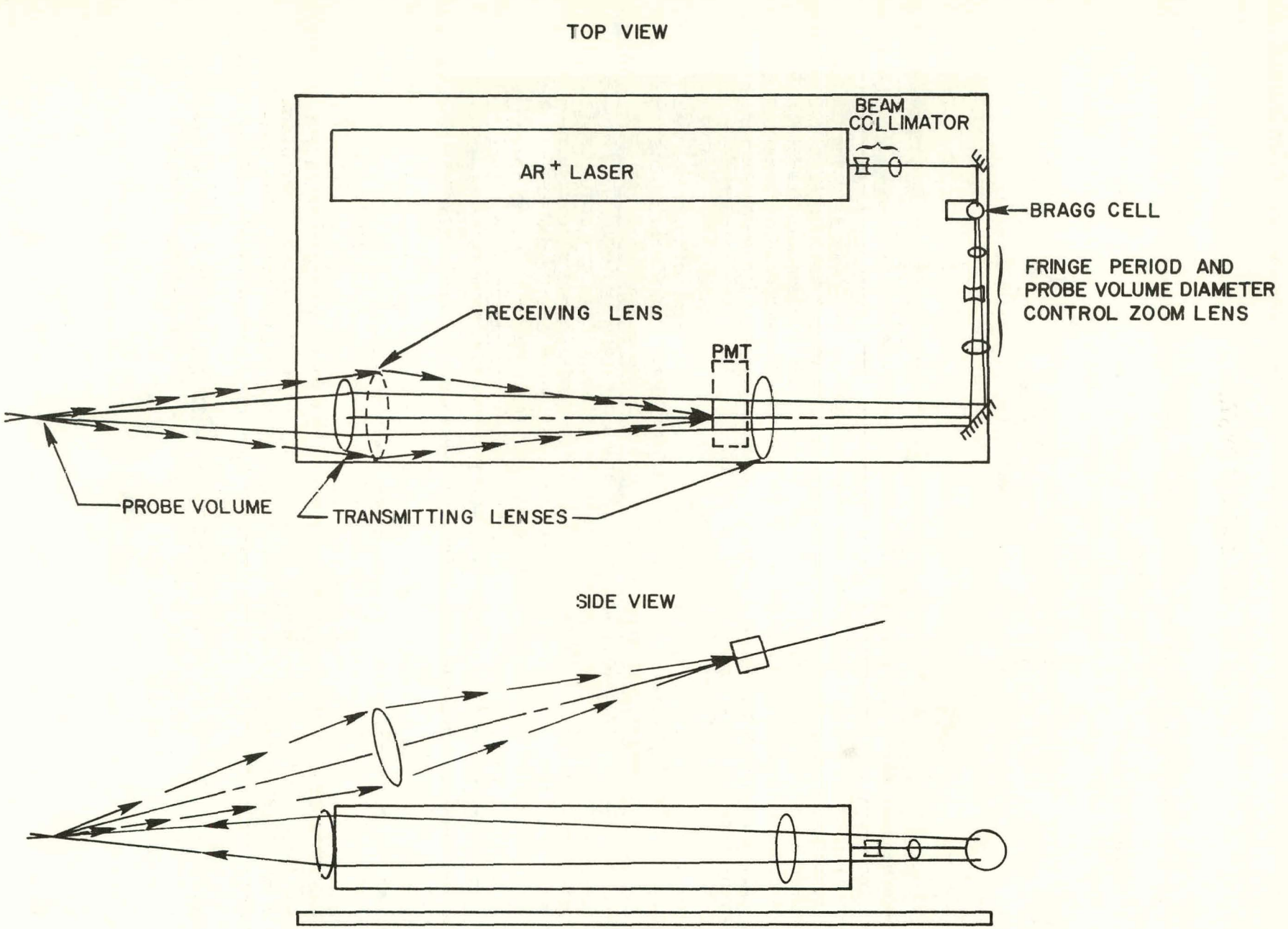

Figure 13. Schematic of Laser Vector Velocimeter System

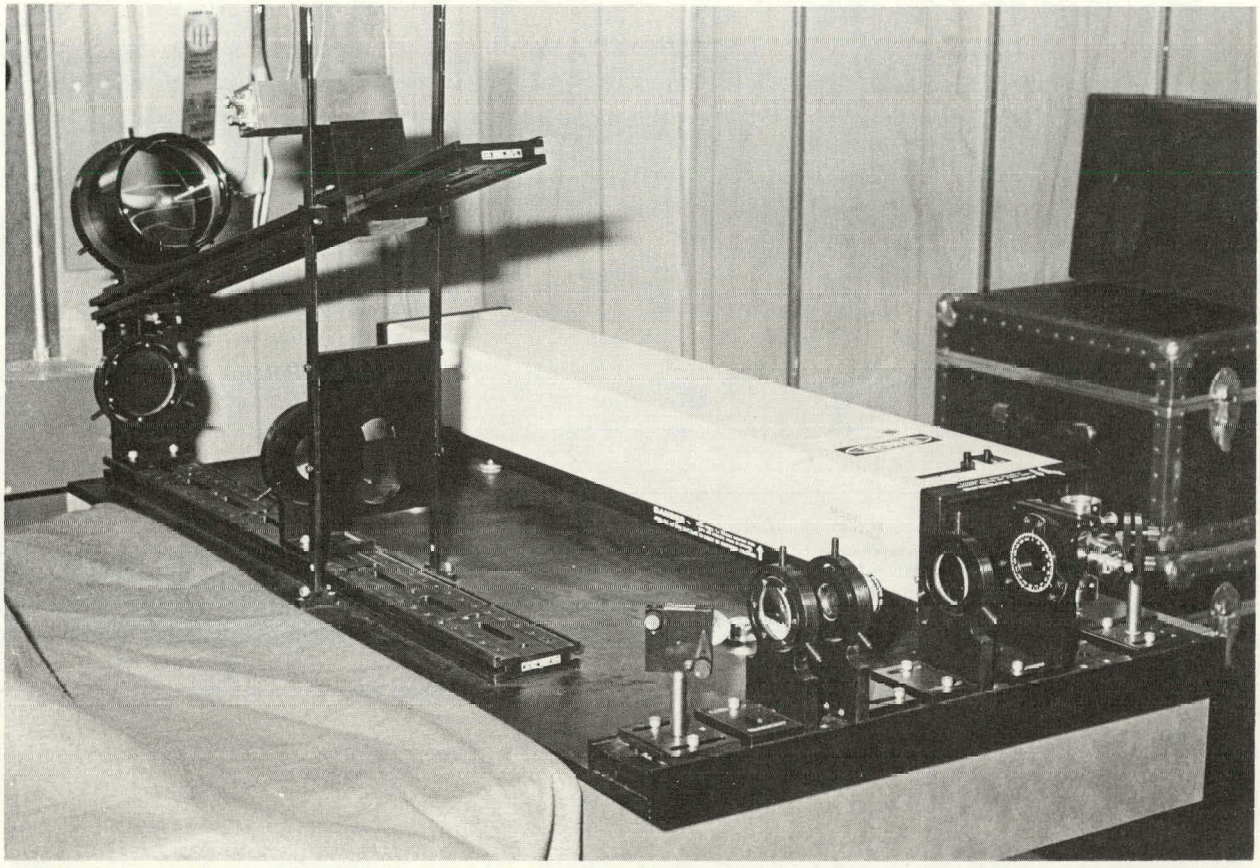

Figure 14. Photo of Assembled LV Optical System

3.1.3 Signal Processing and Data Reduction Systems

The major components of the signal processing system are shown in Figure 15. The signals generated by the photomultiplier tube are transmitted to the signal separator. This device has been designed and developed by the UTSI Gas Diagnostics Division and is similar in function to an FM radio receiver. First, the velocity components corresponding to each of four possible carrier frequencies are separated and identified. The carrier frequencies correspond to 15, 30, 45, and 60 MHz and correspond to two orthogonal velocity components (15 and 45 MHz) and to two nonorthogonal components (30 and 60 MHz). Secondly, in order to achieve a high signal-noise ratio, the high frequency signals are mixed to a lower frequency which is switch-selectable in 10 KHz steps to 3 MHz. This allows optimization of system accuracy and resolution achieved by thumbwheel switches and filter position settings for each channel. In the present configuration, only the 15 and 45 MHz channels of velocity are measured. The velocity measuring electronics are briefly summarized in Appendix A. After the velocity components have been identified and the proper parameters measured to obtain a vector velocity, the data are in a digital format recorded by a small microprocessor system developed by Cromemco®. Software has been developed to compute the mean and standard deviation of each of the velocity components. When data occur simultaneously in both velocity channels, a two dimensional velocity vector, its magnitude and direction, is computed along with the velocity distribution statistics. An internal clock may also be used to identify individual data point acquisition time to the nearest microsecond. From the data, power spectral densities can be computed using specialized software programs developed in the UTSI Gas Diagnostics Division.

If it is desired to measure particle size in addition to velocity, electronics can be incorporated into the existing system with minimal modification. Figure 16 shows the signal processing and data acquisition systems.

3.1.4 Test Bed for Laser Velocimeter (LV)

Because the LV provides spatially resolved velocity measurements it is possible to measure velocity and turbulence profiles by traversing the LV probe volume across the flow. Therefore, a traverse has been designed around a Brown and Sharpe three axis horizontal milling machine configured to move the laser head and optical system along any of three mutually orthogonal axes. To allow direct measurement of velocity components when traversing the flow, the two component axes measured by the LV were selected as two of the three traverse axes. The traverse was designed to move the laser and optics as one unit so that optical adjustments could be made to form the probe volume by beams intersecting at their waist region (where the wave fronts are planar) thus avoiding non-uniform fringe spacing. The traverse position is displayed digitally by a mill bed motion monitor having an accuracy of 0.00127 cm, so that the spatial isolation of the LV measurements is limited by the size of the LV probe volume and not the traverse.

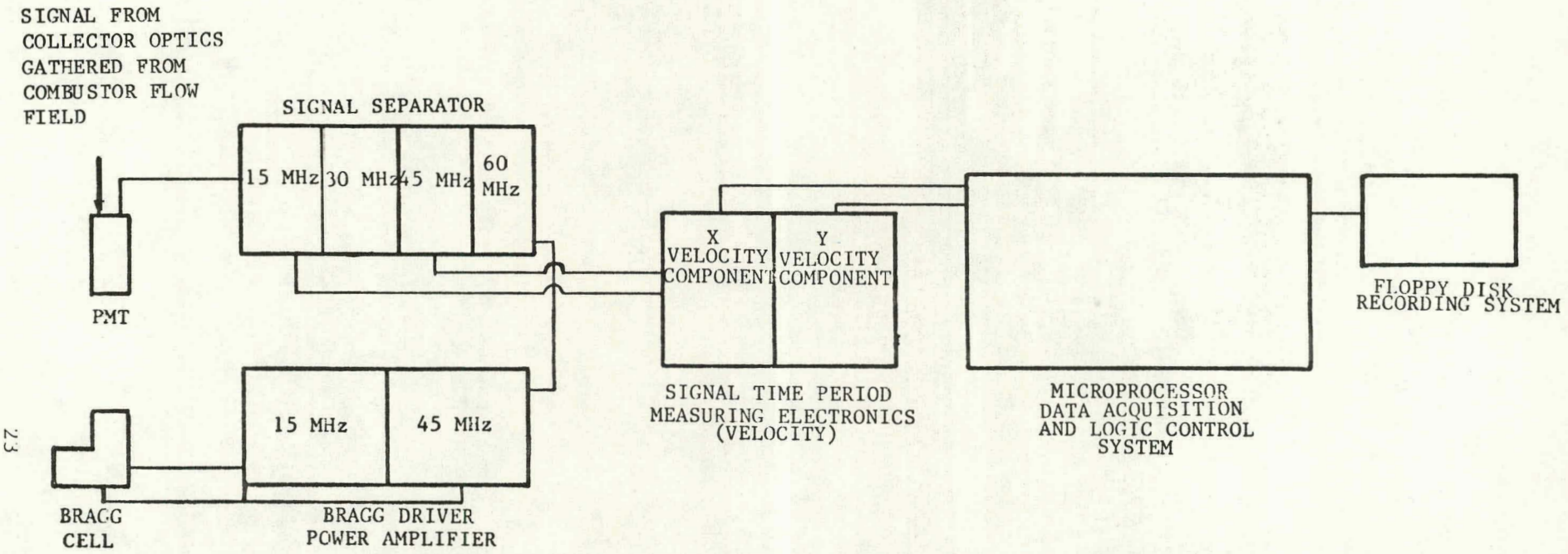

Figure 15. Schematic of Signal Processing System

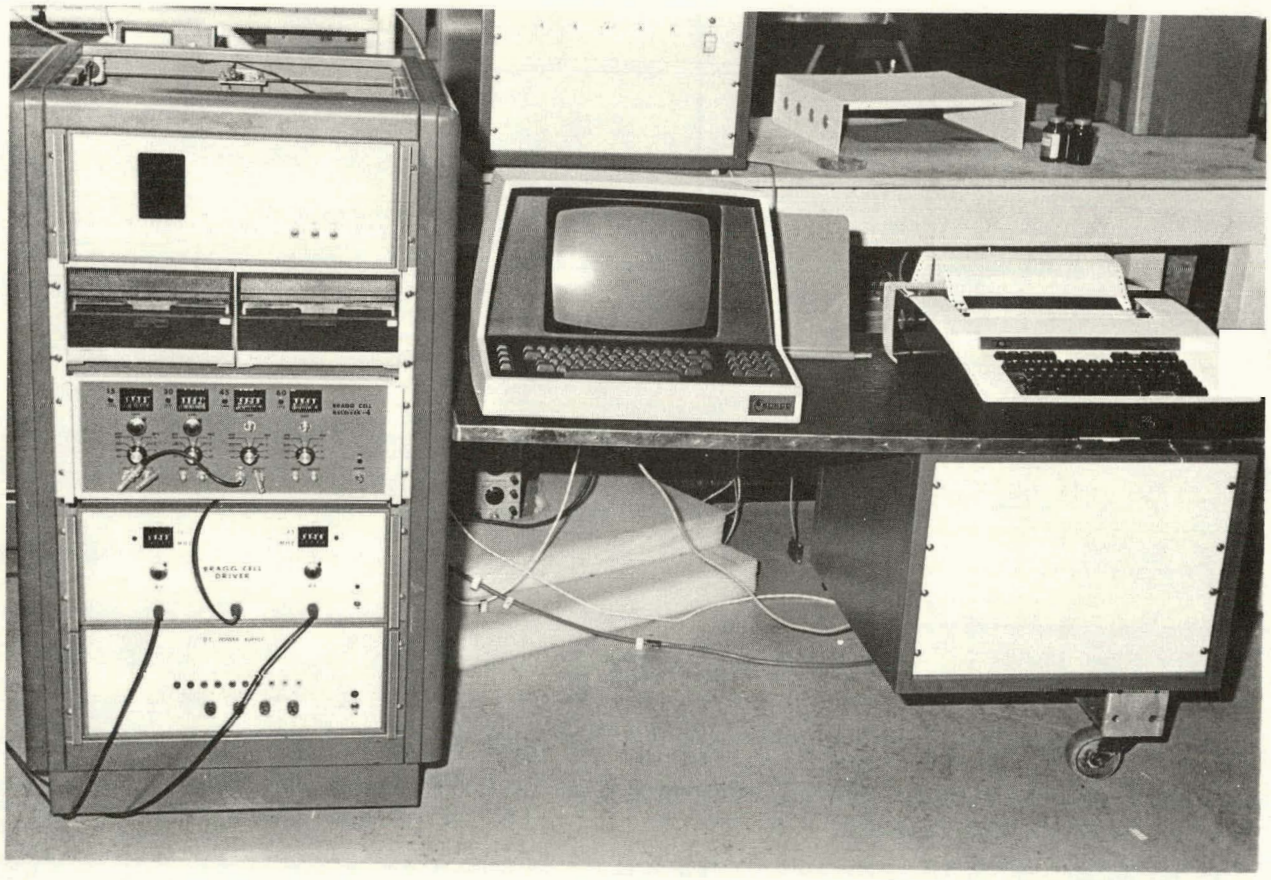

Figure 16. Photo of Signal Processing, Analysis and Display Hardware

3.2 Flow Visualization Techniques

3.2.1 Bubble Generators

Two methods for injecting tracer bubbles into the flow have been utilized. One method is to inject air bubbles into the flow, at desired locations, through hypodermic-needle-tipped probes. A small tube diameter is necessary to make small enough bubbles. Small bubbles, of the order of 2 mm, provided optimum results. They are large enough to be visible and reflect light, and yet small enough to follow the flow reasonably well. The hypodermic tip must be smaller than 2 mm because the air expands from the tip when it forms the bubble.

The other method of flow visualization is to generate hydrogen bubbles on the surface of fine wires strung across the flow. Voltage is applied to the wires and hydrolysis releases hydrogen gas on the wire surface. The gas forms small bubbles and these are swept off the wire by hydrodynamic forces. The hydrogen bubble generation method is applicable primarily in the very low velocity regimes. The bubbles created are not large enough nor are there enough of them to be visible in the turbulent flow downstream of the plate.

3.2.2 Dye Injection

Another type of flow visualization tried was dye injection. Colorful dyes are injected into the flow at desired locations through hypodermic-needle-tipped probes. The flow near the injector location is easily observed because of the dye in the flow. However, the turbulence in the combustor simulator downstream of the plate is so intense that after about ten oxidizer jet diameters downstream of the plate the flow becomes almost uniform in color. Nevertheless, the dye injector method is useful for probing and visualizing local regions in the combustor.

4.0 RESULTS AND SYSTEM STATUS

4.1 Installation and Setup

A model of the CFFF primary combustor is currently being investigated. The flow system and the laser velocimeter measurement system are fully operational. Currently, a variety of different disperser plate models are being investigated to discover the aerodynamic flow fields generated by different disperser plates. At present, the cold flow modeling is limited to completion of the investigation of the existing version of the CFFF combustor with single, centrally located coal injection. Even for this simple configuration, some interesting results have been obtained.

Figure 17 shows a sketch of three different disperser plates that have been tested. Each contains only a single row or ring of holes in a circumferential pattern. Each disperser plate has the same number of holes, and the holes are all the same size. The difference in these disperser plates is that the radius of the ring of holes is increasing, from plate 1 to plate 3.

r = Radius of holes

R = Radius of plates

Plate 1

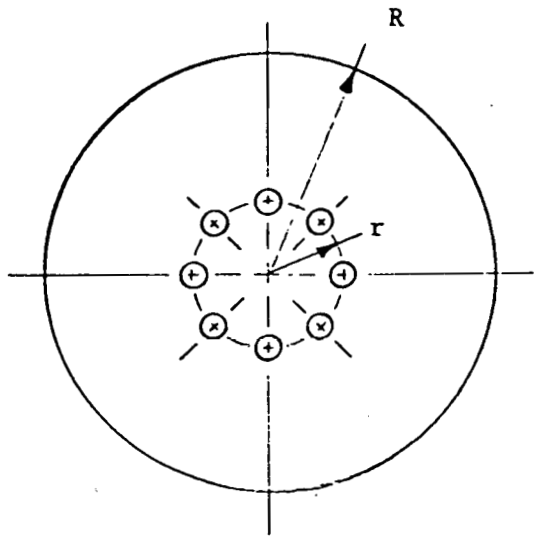

$\frac{r}{R} = 0.33$

Eight holes @
1.19 cm dia. for
8.58 cm^2 total area, or
2.57% plate porosity.

Plate 2

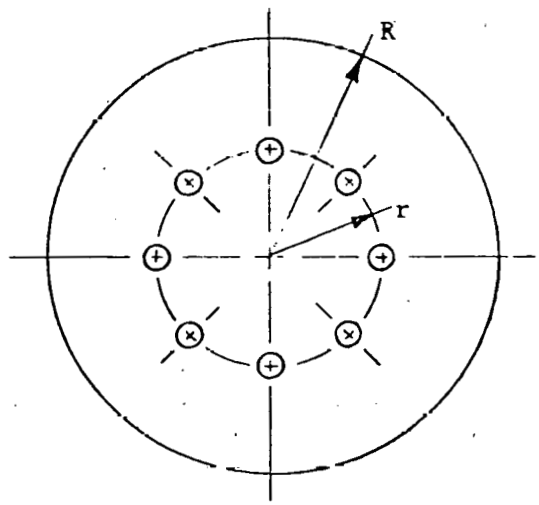

$\frac{r}{R} = 0.50$

Plate 3

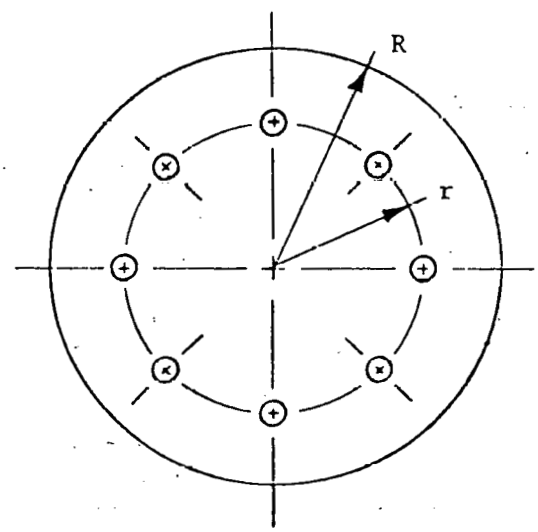

$\frac{r}{R} = 0.66$

Figure 17. Plate Designs for the Preliminary Experimental Investigation

4.2 Results from Cold Flow Testing

In order to explain the measured features of the flow field, it is necessary to examine the measurements in comparison to theoretical predictions.

To illustrate the theoretical aerodynamic behavior of this type of combustor, Figure 18 presents the streamlines and axial velocity components that were computed for a case where the combustor flow field was treated as an axisymmetric, two-dimensional flow. It is important to observe from Figure 18 that the distinguishing features of this type of combustor are two zones of recirculating fluid. The zones are the regions where flames are stabilized by aerodynamic processes and the geometries, strengths and temperature distributions control the combustor operation. These zones are the outer recirculation zone near the walls of the combustor and the inner recirculation zone on the centerline of the combustor.

The laser velocimeter studies of the flow fields generated by the three plates revealed that even geometrically simple injection configurations produced complex flow patterns. Figure 19 shows the mean velocity vector field in a vertical plane passing through the combustor for plate 1. Comparison of the general streamline pattern from the velocity vectors with the two-dimensional calculated streamline pattern of Figure 18 results in an interesting difference. In the measured flow field, there is no central recirculation zone. In the calculated flow field, fluid is backflowing on the centerline toward the disperser plate, whereas measured velocity vectors in this region are directed downstream toward the nozzle. The conclusion is that the measured flow field is three-dimensional with some, but not all, of the features of a two-dimensional flow. The explanation of Figure 19 is provided in Figure 20. Figure 20 is a survey of the same flow as shown in Figure 19, but in a plane of the combustor between the holes of the disperser plate. Careful comparison of Figures 19 and 20 reveals that the fluid from the outer wall recirculation zone passes down between the holes in the disperser plate and eliminates the central recirculation zone. This phenomenon was discovered for two of the single- row-of-holes disperser plates. Figures 21 - 24 show the vector velocity field measured for the other plates taken in different planes cutting the combustor. Note that for plate No. 3, a central regime of back flow does exist, as two-dimensional theory requires. For this case, the between-hole survey showed fluid flowing up between the holes and then coming down farther out. This produces an interesting three dimensional, cellular flow pattern in the combustor model.

In the Coal Fired Flow Facility (CFFF), the disperser plate has up to three rows or rings of holes available for oxidant injection. The holes can be individually opened or plugged to generate variable hole patterns for oxidant injection. The current version of the CFFF combustor has a disperser plate with two unplugged rings of holes, Figures 3 and 10.

The model of the CFFF disperser plate, Figure 10, was tested in the Cold Flow Modeling Facility. The velocity vector flow field obtained by laser velocimetry is shown in Figure 25. As can be seen, this plate also generates a three-dimensional flow field which has a small or negligible

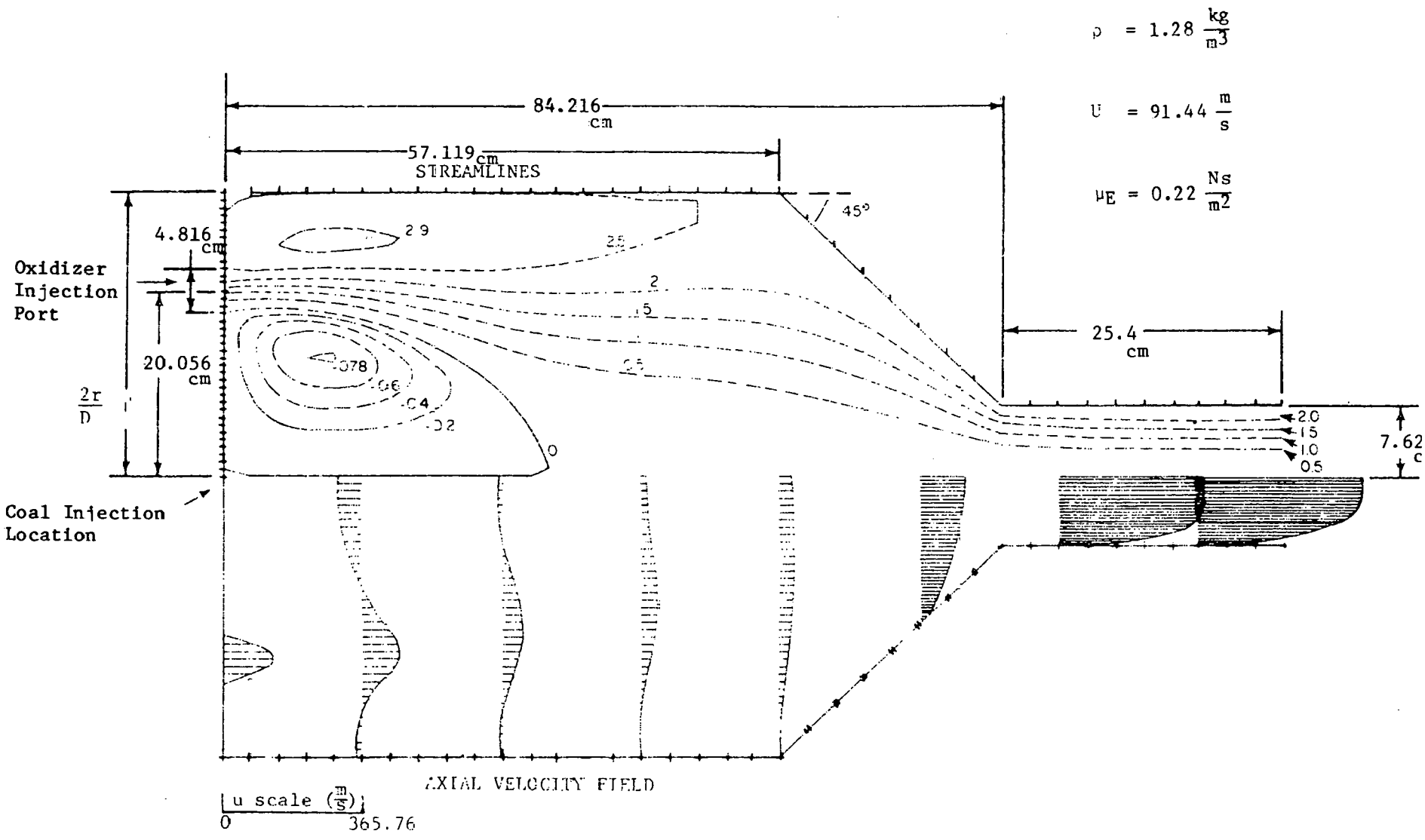

Figure 18. Theoretical Calculation of Flow Field Inside the UTSI Design Pulverized Coal Combustor Single Oxidizer Injector Ring

VER. TRAV. PLOT, PLATE 1, FLOW RATE = 0.002839 m^3/sec or 2.839 liters/sec

JETS ON RADIUS = 3.493 cm, ORIENTATION = 0.0 DEG

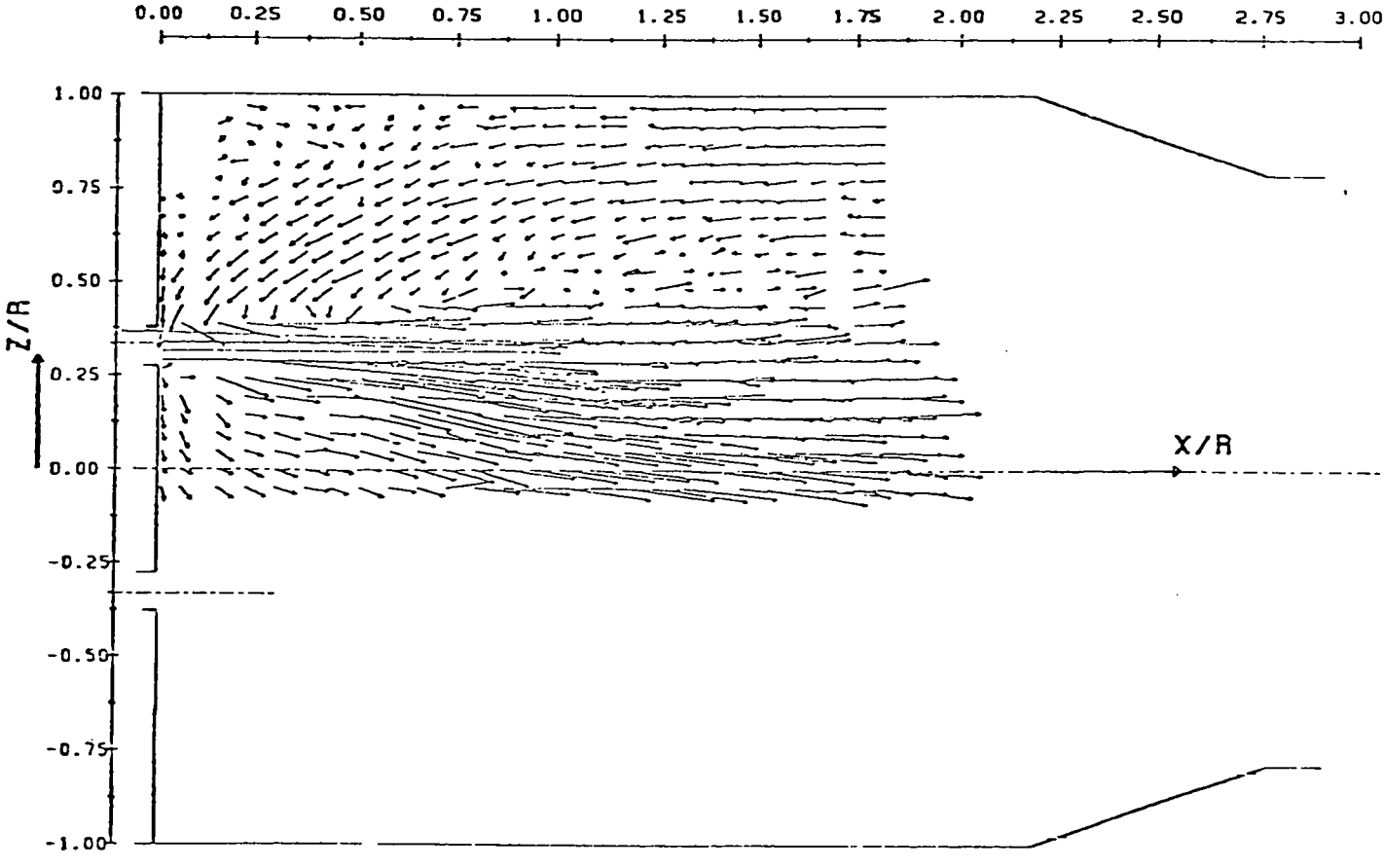

Figure 19. Velocity Field in the Plane of an Oxidant Jet
(Plate 1, Figure 17)

VER. TRAV. PLOT, PLATE 1, FLOW RATE = 0.002839 m^3/sec or 2.839 liters/sec

JETS ON RADIUS = 3.493 cm, ORIENTATION = 22.5 DEG

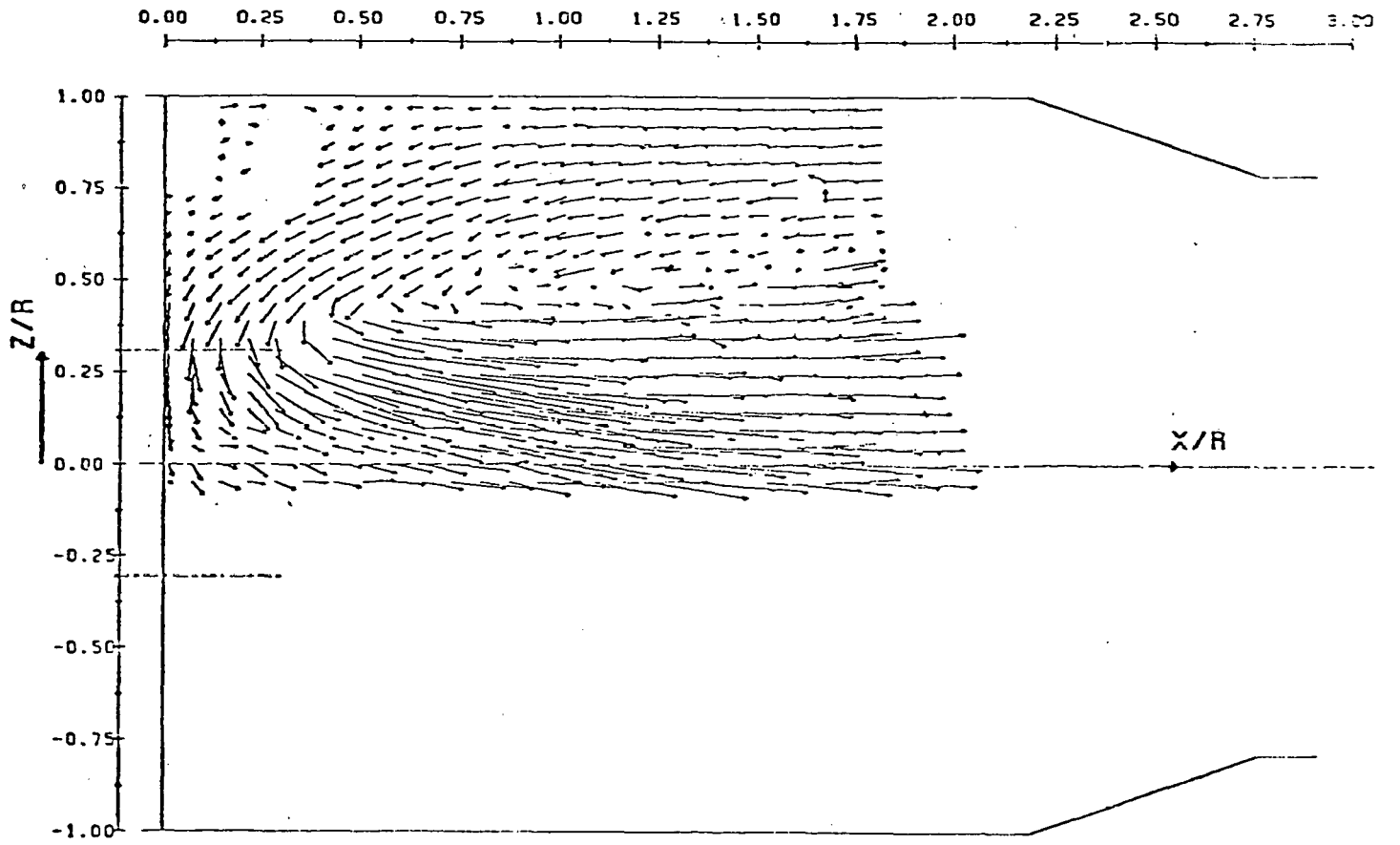

Figure 20. Velocity Field in Plane Between Oxidant Jets
(Plate 1, Figure 17)

VER. TRAV. PLOT, PLATE 2, FLOW RATE = 0.002839 m^3/sec or 2.839 liters/sec

JETS ON RADIUS = 5.232 cm, ORIENTATION = 0.0 DEG

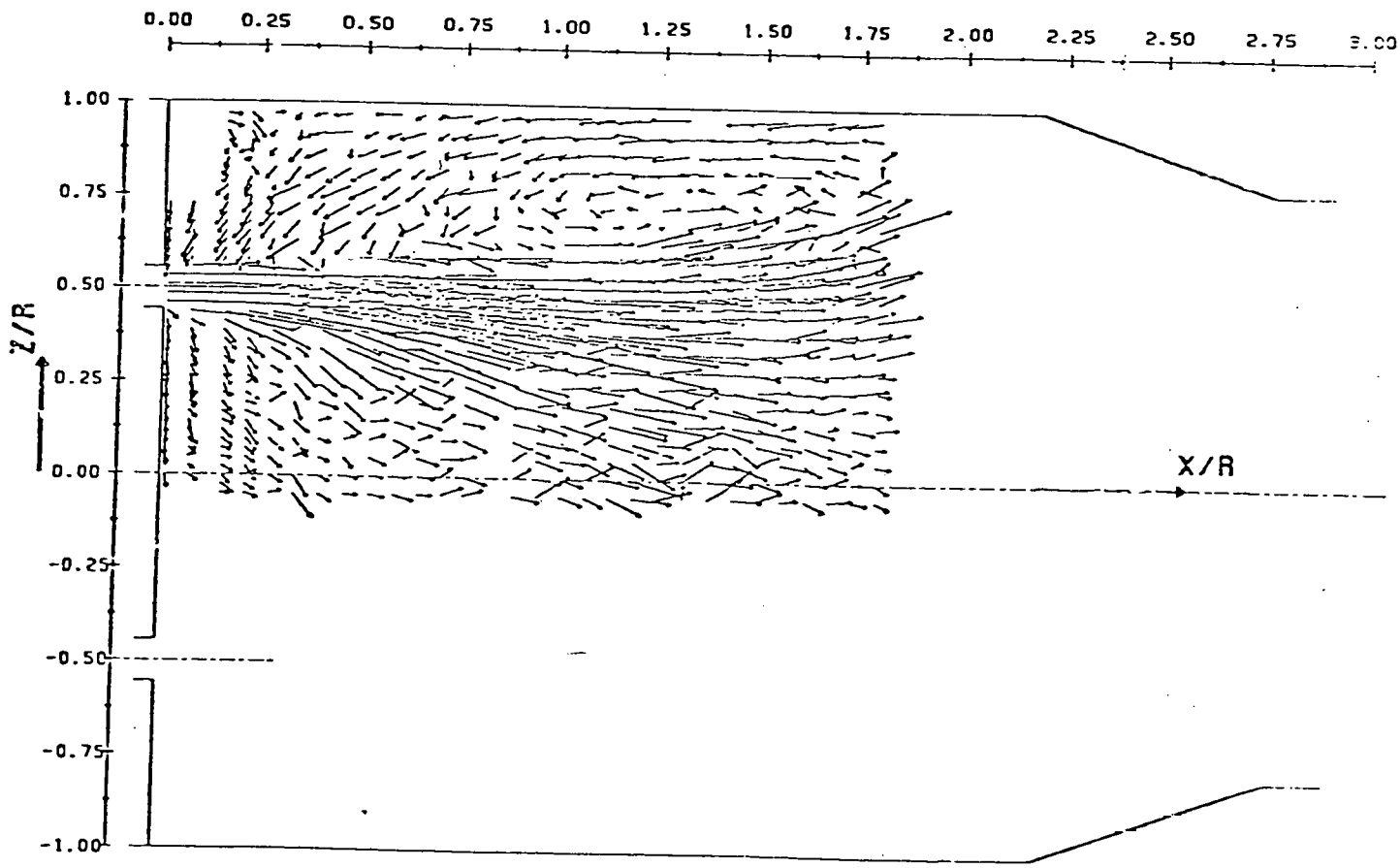

Figure 21. Velocity Field in the Plane of an Oxidant Jet
(Plate 2, Figure 17)

VER. TRAV. PLOT, PLATE 2, FLOW RATE = 0.002839 m^3/sec or 2.839 liters/sec

JETS ON RADIUS = 5.232 cm, ORIENTATION = 22.5 DEG

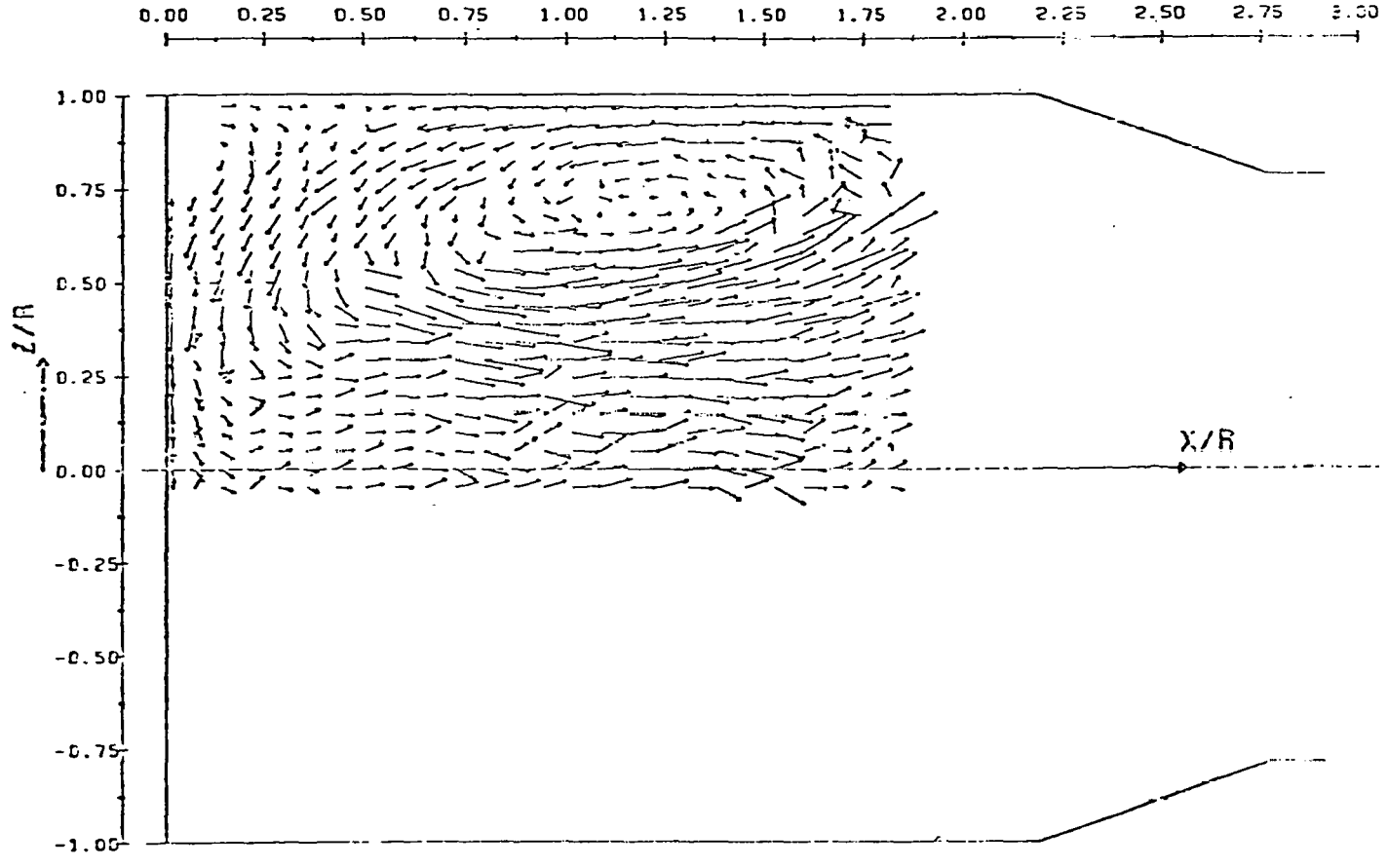

Figure 22. Velocity Field in a Plane Between the Oxidant Jets (Plate 2, Figure 17)

VER. TRAV. PLOT, PLATE 3, FLOW RATE = 0.002839 m^3/sec or 2.839 liters/sec

JETS ON RADIUS = 6.985 cm, ORIENTATION = 0.0 DEG

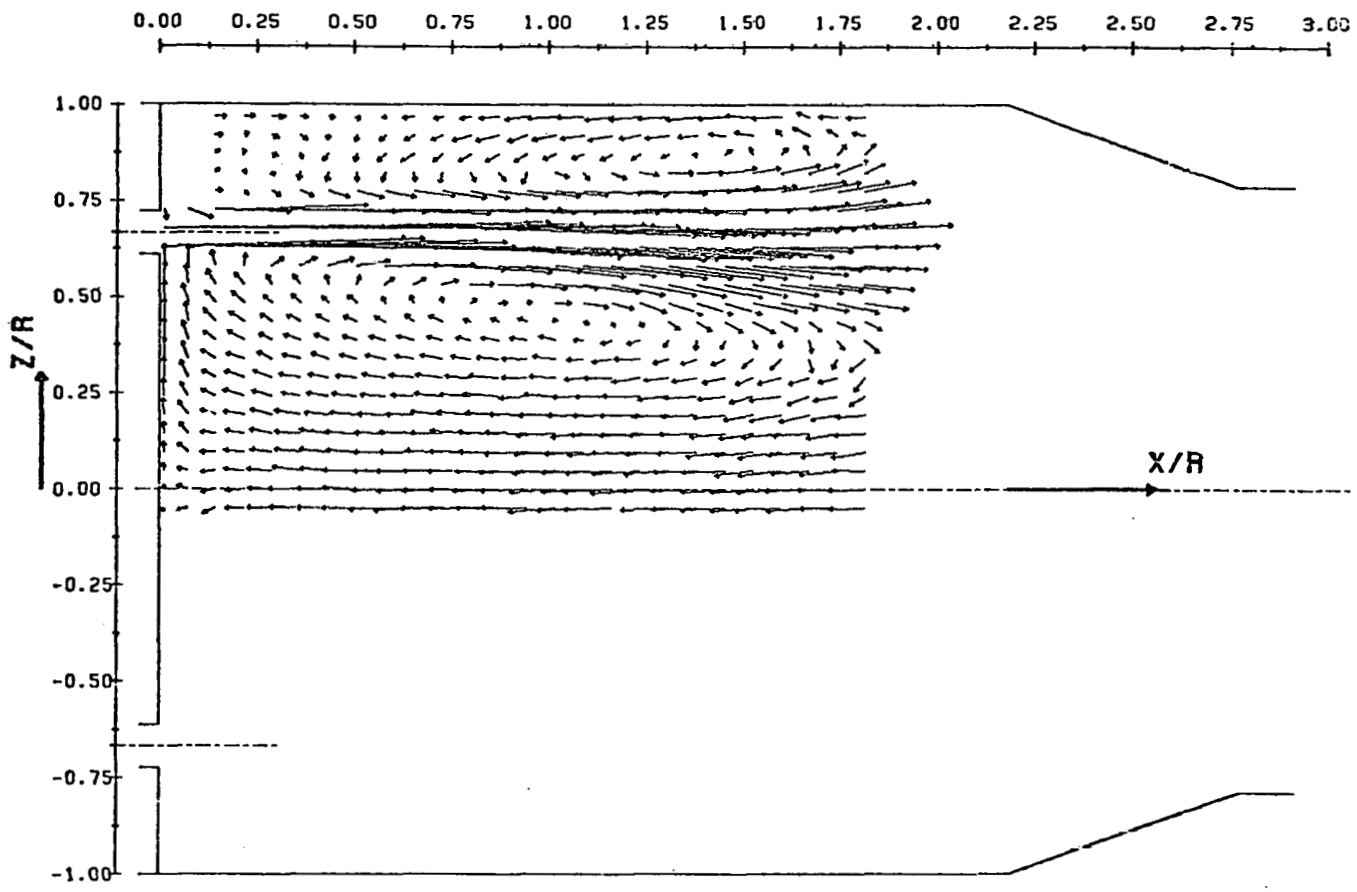

Figure 23. Velocity Field in the Plane of an Oxidant Jet
(Plate 3, Figure 17)

VERTICAL TRAVERSE VELOCITY VECTOR PLOT, PLATE 3, FLOW RATE = 0.002839 m^3/sec or 2.839 liters/sec

JETS ON RADIUS = 6.985 cm, ORIENTATION = 22.5 DEG

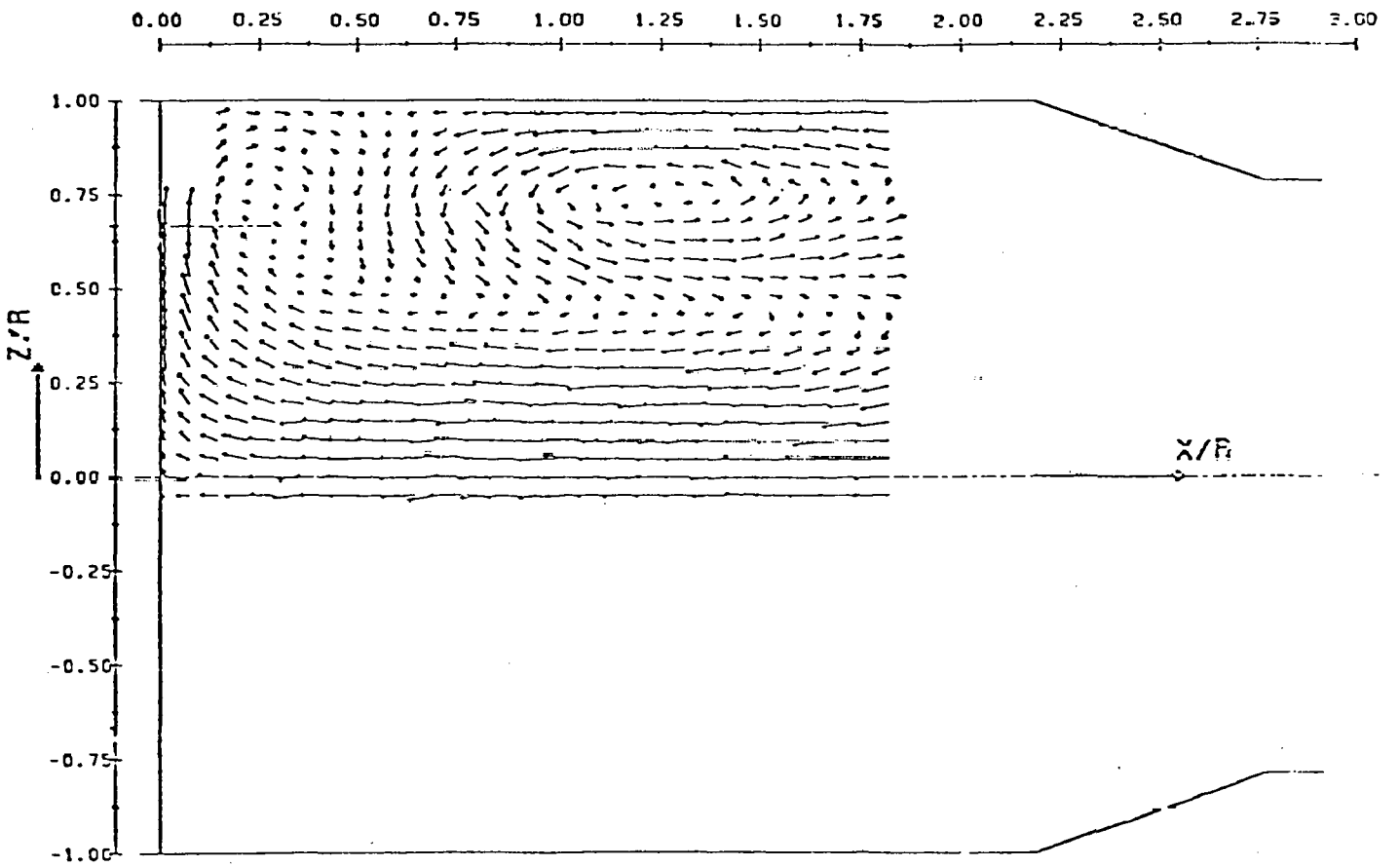

Figure 24. Velocity Field in the Plane Between Oxidant Jets (Plate 3, Figure 17)

VERTICAL TRAVERSE VELOCITY VECTOR PLOT, 32 JETS, FLOW RATE = 0.002839 m^3/sec or 2.839 liters/sec

JETS ON RADIUS = 3.886 & 5.055 cm, ORIENTATION = 0.0 DEG

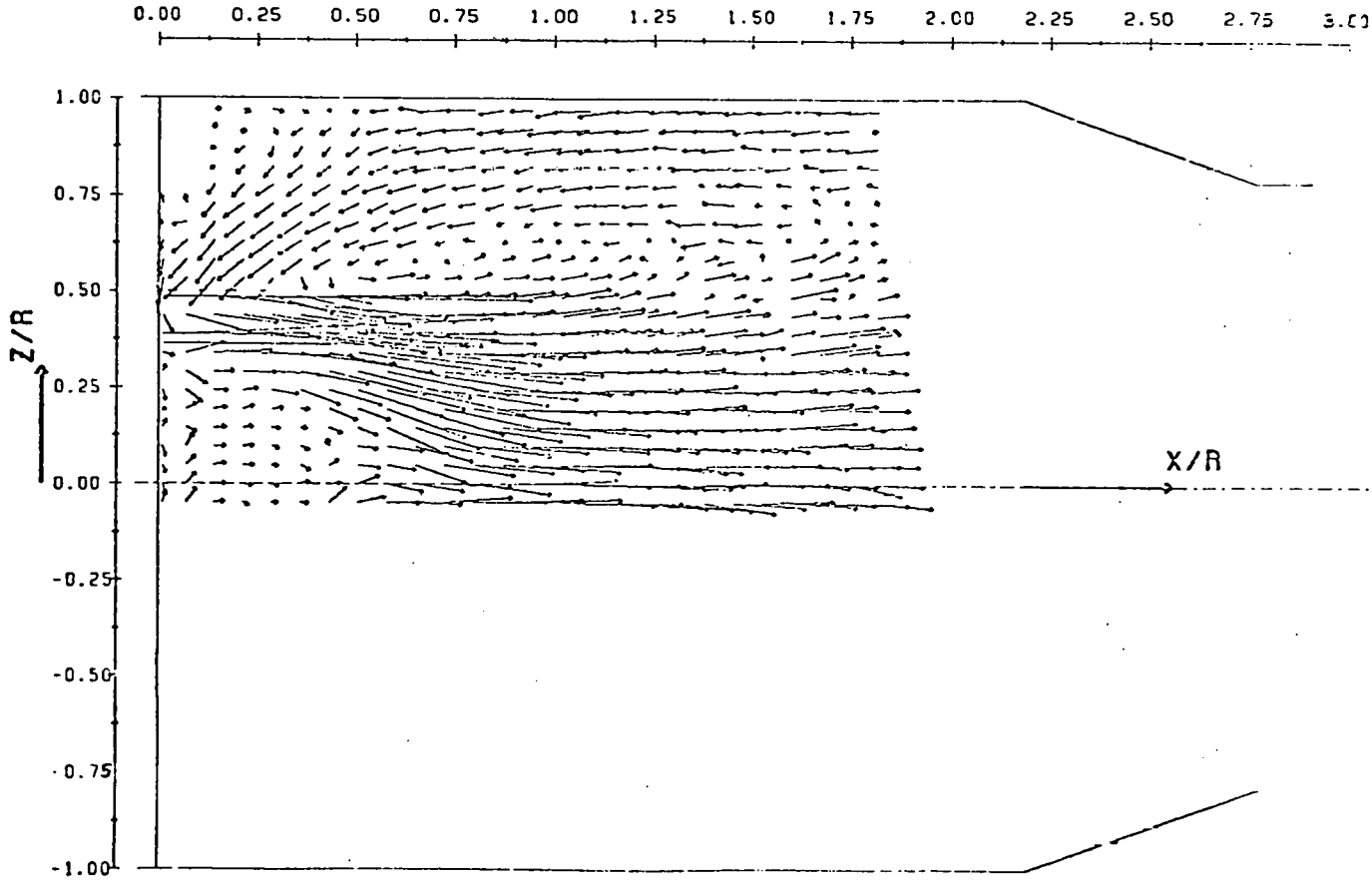

Figure 25. Velocity Field of the CFFF Disperser Plate; (Figure 10) With Two Rows of Injector Holes, in the Plane of an Oxidant Jet

regime of recirculation on the centerline. Again, this effect is caused by the fluid from the outer recirculation zone passing down between the holes into the central region of the combustor, thus blowing off the central recirculation region.

4.3 Implications of the Experimental Results

Several implications result from the experimental results that affect combustor performance and performance evaluation. First, the data suggest that in the CFFF combustor the central coal injection system injects coal, not into a recirculation zone as predicted by two-dimensional theory, but, into a downstream directed flow, similar to a centralized plug flow. Operation of the combustor as an entrained flow, fully stirred reactor is not probable, therefore, and at best with existing injection systems for oxidizer and fuel, it operates as a partially stirred reactor.

Second, the data show that an analytical or numerical theoretical model of the combustor must be three-dimensional to accurately predict temperature profiles, velocity profiles, and gas species concentration profiles. Thus, since computer models of the combustor, (which can be used to generate the anticipated, complex combustor scaling rules) must be fully three-dimensional, they will be expensive to formulate and to operate.

Third, any changes in disperser plate configuration, which change fuel or oxidant injection patterns, should be experimentally evaluated in a cold flow model configuration first because of the complex nature of the flows generated by even relatively simple disperser plate geometries (i.e. hole patterns). Then, if cold flow operation is satisfactory, a new, actual CFFF disperser plate configuration can be hot tested.

4.4 Problems Encountered in Laser Velocimeter Research

Several problems were encountered in setting up this facility for the research effort. Many of these problems are very familiar ones such as metering the flow of the working fluid, water, in order to establish the correct mean velocities, turbulence and flow Reynolds numbers. The problems specific to the operation of the laser velocimeter include:

1) developing techniques for focusing the beams at known positions in the flow, which generates the probe volume at known spatial positions.

2) eliminating random air bubbles from the water flow so that a large number of bubbles of very uniform size could be generated in the system and used as "seed" or scattering centers for the LV beams.

3) arranging the photomultiplier tube and light collection optics in a back scatter arrangement that permits optimal signal recovery.

4) developing software for the microprocessor controlled data acquisition system that permits data with acceptable statistical confidence to be obtained with reasonably manageable data sample sizes, and at fast enough rates.

All of the problems have been resolved. The discussion of the problems is outside the scope of the present report. Some of the problems are discussed in detail in reference 5.

5.0 STATUS OF RESEARCH FACILITY

The Cold Flow Modeling Facility is fully operational. Various fluid dynamic research programs have been conducted there, all directly applicable to CFFF performance evaluation and improvement. For example, reference 5 is a description of research conducted to evaluate the performance of the CFFF secondary combustor air injection and mixing system. Problems in applying the LV to both seeded air and water flows have been resolved, and current LV measurements occur on a routine basis. The Cold Flow Modeling Facility is a powerful tool for investigating the fluid dynamic behavior of both small and large scale operations.

REFERENCES

1. Durst, F. and Stevenson, W. H., "Properties of Focused Laser Beams and the Influence on Optical Anemometer Signals," Proceedings of the Minnesota Symposium on Laser Anemometry, University of Minnesota, pp. 373-388, October, 1975.

2. Chriss, D. E., "An Experimental Investigation of Ducted, Reactive, Turbulent Jet Mixing with Recirculation," AEDC TR-77-56, September, 1977.

3. Smith, G. D. and Giel, T. V., "An Experimental Investigation of Reactive, Turbulent, Recirculating Jet Mixing," AEDC TR-79-79, May, 1980.

4. Bray, K. N. C., "Equations of Turbulent Combustion, I Fundamental Equations of Reacting Turbulent Flow," University of Southampton, Department of Aeronautics and Astronautics, AASU Report No. 330, October, 1973.

5. Foote, J. P., "A Cold Flow Model Study of Turbulent Mixing in a Secondary Combustor," Master of Science Thesis, The University of Tennessee, Knoxville, Tennessee, December, 1982.

APPENDIX A

Laser Velocimeter Burst Processors and Signal Visibility Analyzers

I. LV Burst Processors

Whenever a particle passes through the probe volume of a laser velocimeter (LV) system, it scatters laser light from the interference fringes. The intensity of this scattered light is coverted into an electrical signal by a photomultiplier tube (PMT). This PMT output signal consists of a higher-frequency Doppler component added to a lower-frequency pedestal component. The frequency of the Doppler component indicates the velocity of the particle which produced it. One way to measure the Doppler frequency of individual signal bursts is to use a burst processor, which basically operates like a frequency counter in the time period mode.

The block diagram of the basic burst processor shown in Figure A-1 illustrates its operating principles. Shown below the system's block diagram is a sample timing chart. The amplified burst signal from the PMT goes into a zero-crossing detector (ZCD) after a high-pass filter has removed the pedestal component. The ZCD is basically a Schmidt trigger which compares its input to a threshold voltage. The ZCD's digital output is high only when its input exceeds the threshold voltage. Therefore, the frequency, f, of the ZCD's output is

$$f = 1/\tau = V_Y/\delta \qquad (1)$$

where V_Y is the particle's velocity component perpendicular to the interference fringes having the spacing δ.

This output serves as the clock signal for a fringe counter which is preset to count N pulses. While the fringe counter is advancing, it produces an output pulse of length $N\tau$ which is used to enable a clock counter. As long as the fringe counter's output is high, the clock counter counts pulses from a high-frequency reference clock. After the fringe counter's output returns low, the clock counter contains a number, n, which represents the amount of time required for a particle to cross N interference fringes. The particle's velocity perpendicular to the fringes is then determined from

$$V_Y = N\delta f_c/n \qquad (2)$$

where f_c is the frequency of the reference clock.

This simple burst processor is theoretically acceptable, but in practical applications where the ZCD input is a noisy, random signal, it would not perform well. Therefore, several data validation features need to be incorporated into the actual processor design.

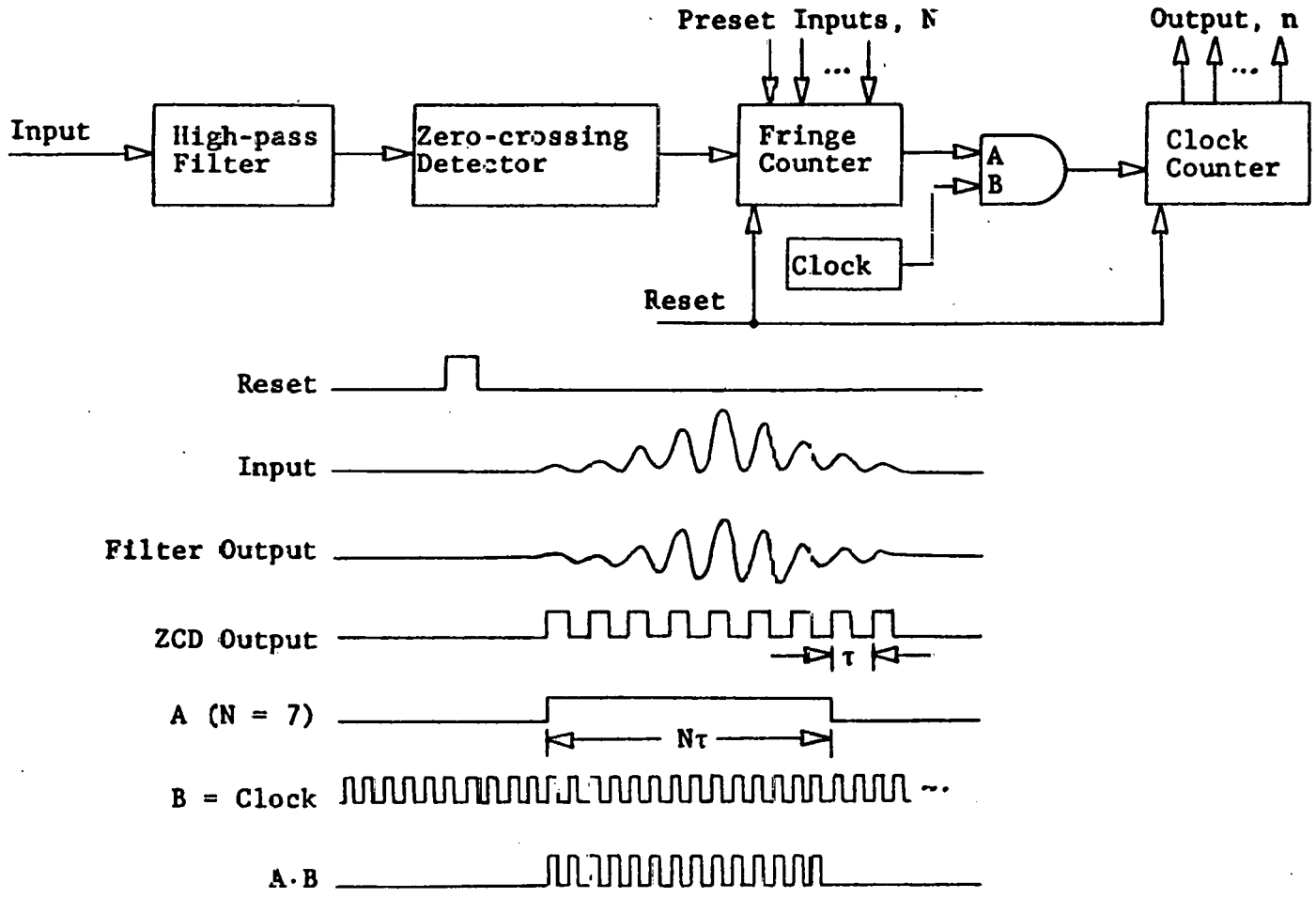

Figure A-1 Basic Doppler Burst Processor

One type of error may be caused by relatively large particles passing through the probe volume. These particles tend to lag behind the flow and produce erroneously low velocity measurements. Since low velocities correspond to low signal frequencies, it is possible to reject these measurements by using a high-pass filter. A digital high-pass filter may easily be implemented in the burst processor. For a given fringe count, lower-frequency Doppler input signals will cause larger counts to accumulate in the clock counter. By comparing the clock counter output to a number stored in a latch, it is possible to detect when the processor is attempting to measure a burst with too low of a Doppler frequency.

A measurement error would also occur if the burst processor's input signal briefly disappeared while a measurement was being made. This could easily be caused by one particle leaving the probe volume shortly followed by another particle entering it. The final count thereby accumulated in the clock counter would be erroneously high. As a result, the velocity would appear to be lower than it truly was.

One way to avoid this error is to test the input signal for periodicity. Such a test may be performed using two sets of fringe counters and two sets of clock counters. One fringe counter is preset for a LONG count, N_L, while the other is preset for a SHORT count, N_S, where N_L is greater than N_S. After completion of both fringe counts, the corresponding LONG and SHORT clock counts are n_L and n_S respectively. The aperiodicity, ε, can be computed from

$$\varepsilon = 1 - \frac{N_L\ n_S}{N_S\ n_L} \tag{3}$$

A periodic signal would produce an aperiodicity of zero since the ratio N_L/N_S would equal the ratio n_L/n_S (neglecting digitization errors). However, when the ZCD signal temporarily drops out, n_L/n_S assumes a value different from N_L/N_S, and the aperiodicity increases. Test readings with an aperiodicity exceeding a preset limit would be considered invalid.

An example is shown in Figure A-2 where the ZCD output has one missing cycle. This and all other timing diagrams have dotted lines to indicate signal level changes which depend upon each other. The LONG and SHORT signals are the fringe counter outputs which gate clock pulses into their respective clock counters. The N_L and N_S fringe counts are 4 and 3 respectively, while the resulting n_L and n_S clock counts are 10 and 8 respectively. Thus, the aperiodicity given by Equation (3) is 6.7 percent.

Another common problem with LV signals is the loss of a burst signal before the fringe counts are complete. This problem, known as signal dropout, will produce one of two actions. If a second burst soon starts, the fringe counts will be completed, but the erroneous clock counts will later be discarded by the periodicity test. Otherwise, if the fringe counts are not completed, the clock counters will continue counting until they exceed the digital high-pass filter limit, but this could take a relatively long time. Since signal dropout occurs often, the instrument would waste most of its time either letting the clock counters overrun or computing the aperiodicity of many grossly invalid measurements. The dropout detector illustrated in Figure A-3 minimizes the time required to recover from such conditions.

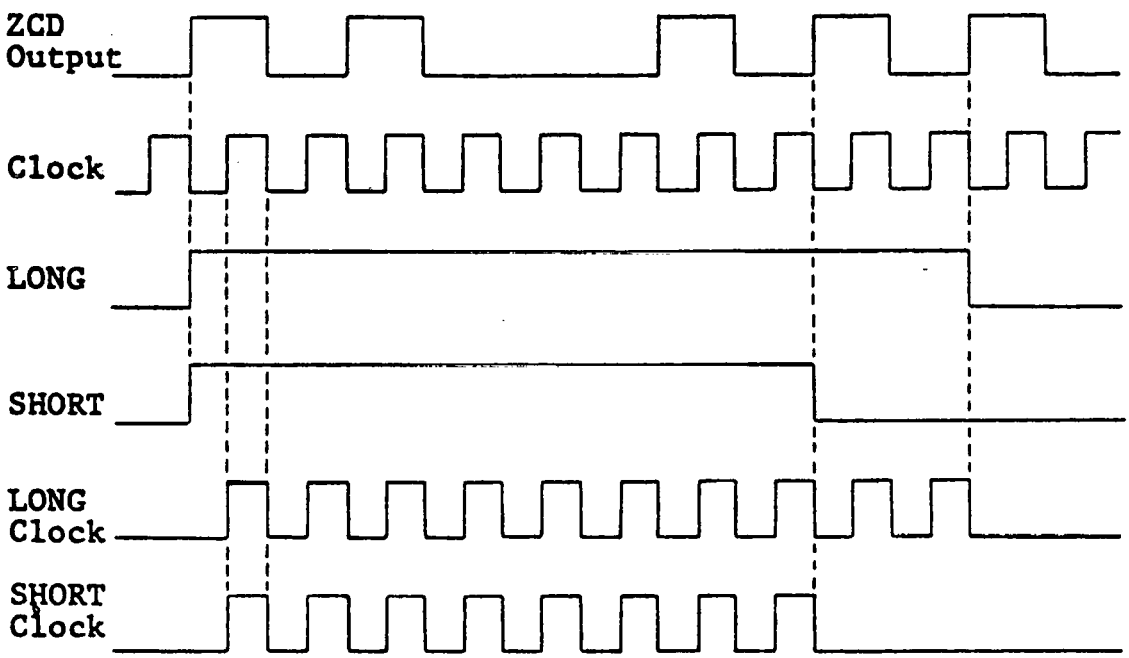

Figure A-2 Timing Diagram for an Aperiodic ZCD Signal

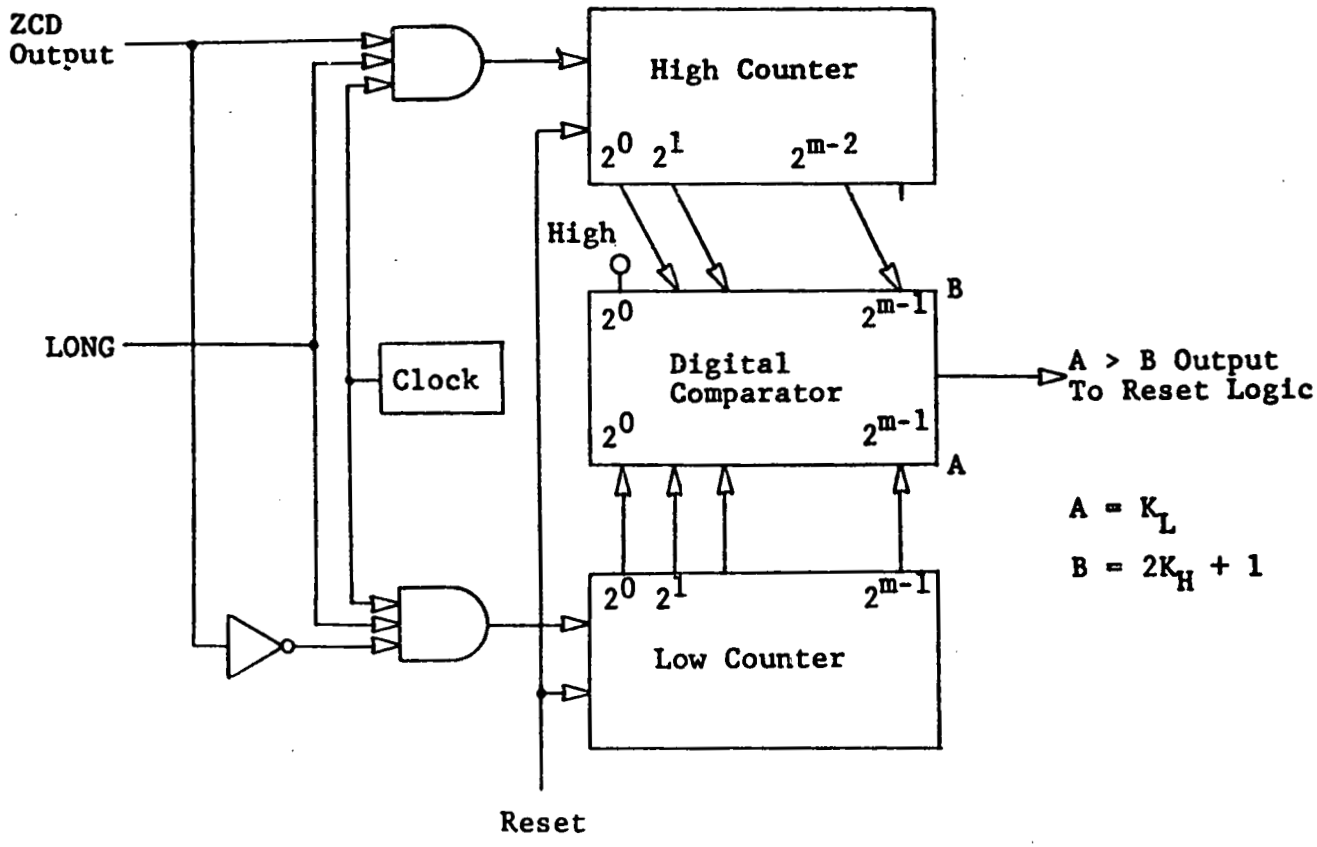

Figure A-3 Block Diagram of Dropout Detector

While the output from the LONG fringe counter is high, the ZCD output alternately gates clock pulses into one of two m-bit counters. For this simple example, assume that the ZCD output frequency is less than the clock frequency. Whenever ZCD and LONG are both high, clock pulses are gated into a counter called the high counter, whereas a low ZCD and high LONG combination gates clock pulses into a low counter. Each output bit from the low counter is compared with the next lower order output bit from the high counter. Thus, K_L is compared to $2K_H + 1$ where K_L is the low count and K_H is the high count.

Suppose that the ZCD output is a relatively symmetrical signal which completes the LONG fringe count. Then, the final values of K_L and K_H are approximately equal, and the digital comparator's output always remains low. Conversely, if signal dropout occurs while LONG is still high, the high count will remain constant while the low count continues to increase. Once K_L exceeds $2K_H + 1$, the comparator's output goes high and activates the reset logic. Hence, the time required to reset the instrument after dropout is approximately equal to the amount of time for which LONG stayed high before dropout.

These error detection circuits, along with other various features, are included in the complete high-speed LV burst processor block diagram illustrated in Figure A-4. Because its operation involves the high-speed manipulation of many binary numbers, this instrument is controlled by a microcomputer. The microcomputer initializes data latches and flip-flops, stores the available data in memory, and later performs the necessary computations. Parameters such as fringe counts, fringe spacing, and clock rate are entered by the operator through a keyboard. Final results may be displayed on a CRT terminal, listed on a printer, or stored on a floppy disk.

Referring to Figure A-4, the burst signal from the PMT is first amplified by a preamplifier to a level which may be transmitted relatively long distances through a coaxial cable. The lower-frequency pedestal component of the signal is removed by an analog high-pass filter. This filter must be manually set by the operator to a frequency just under the expected range of Doppler frequencies. The burst is then transformed into digital pulses by the ZCD which was illustrated in Figure A-1.

In order to avoid starting measurements at the beginning of a burst when the signal-to-noise (S/N) ratio is low, a preset number (1 to 15) of ZCD pulses must first be counted by a precounter. After it has counted the necessary number of pulses, the precounter gates the ACD ouput into the fringe counters. While the LONG and SHORT fringe counts are accumulating, the corresponding clock counters are allowed to count pulses from a reference clock. (High-speed portions of these circuits must be designed using emitter-coupled logic (EDL) devices; the remainder may use transistor-transistor logic (TTL) devices.) Upon completion of the required LONG and SHORT fringe counts (N_L and N_S respectively), the microcomputer is signaled that the clock counts, n_L and n_S, are ready to be processed.

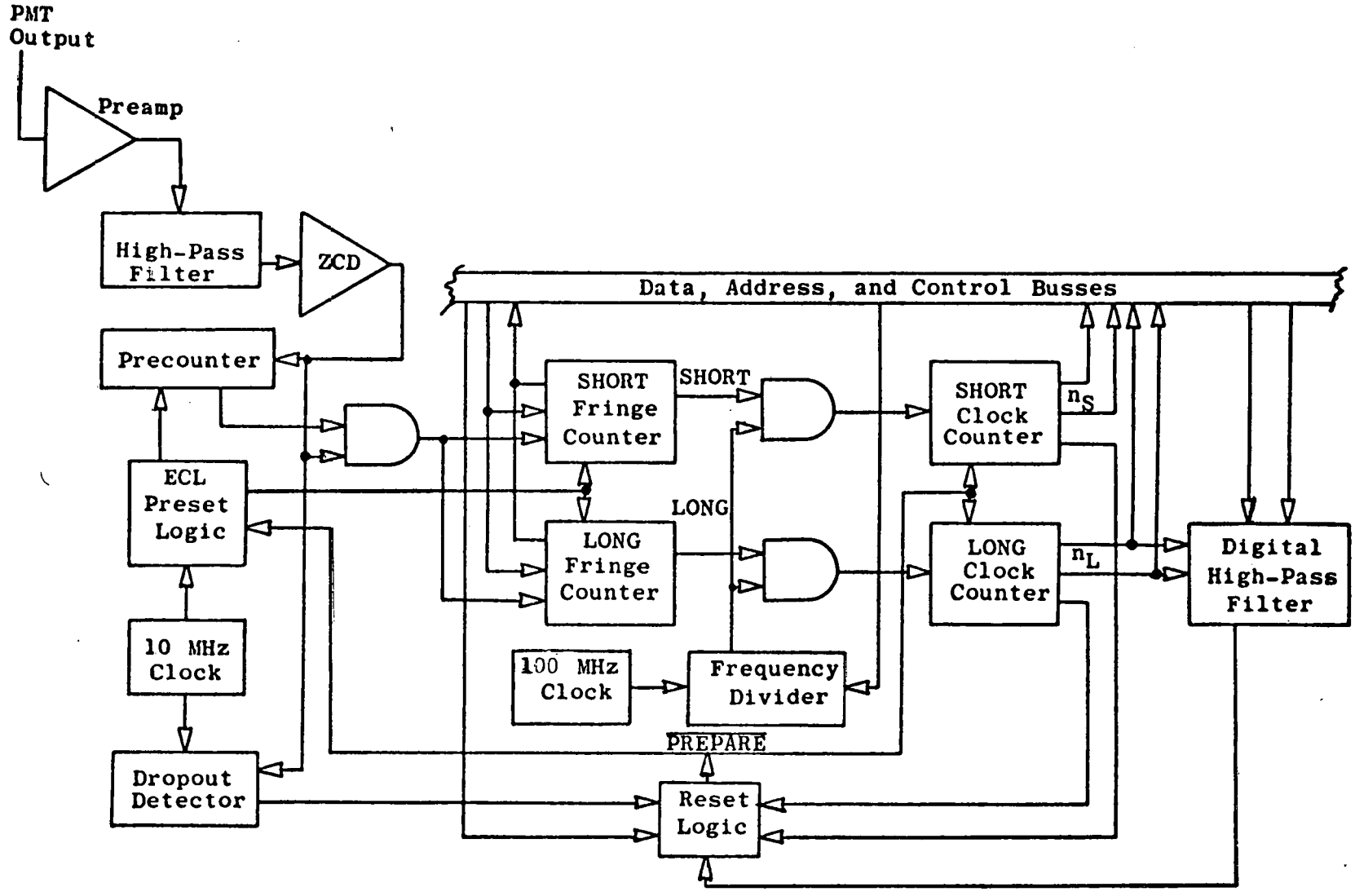

Figure A-4 Complete Block Diagram of LV Processor

The precision of velocity measurements increases as the magnitude of the clock count increases. This indicates the need for a high-frequency reference clock since the fringe count is usually limited by physical constraints on the probe volume. However, if a high-frequency clock is used for the measurement of low-frequency input signals, the clock counters will overflow. The design in Figure A-4 overcomes that dilemma by using a dual-frequency reference clock. Via the microcomputer, one may select either a 100 MHz clock for the measurement of high-frequency inputs or a 10 MHz clock for lower-frequency inputs. The clock rate would normally be set to 100 MHz unless this causes the clock counters to overflow.

Reset logic resets all of the counters and flip-flops in preparation for the next measurement. A reset pulse may be triggered by the digital high-pass filter, the dropout detector, either of the clock counter overflows, or a command from the microcomputer.

II. SIGNAL VISIBILITY ANALYZER

The PMT burst signal contains information about the size of the particle as well as its velocity. This is illustrated in Figures A-5 and A-6 which show particles crossing the interference fringes and the corresponding PMT output waveforms. The particle in Figure A-5, having a diameter much smaller than the fringe spacing, δ, produces a PMT signal with nearly 100% modulation. Figure A-6 shows a particle with a diameter comparable to the fringe spacing. Its corresponding PMT output waveform is not fully modulated like the one in Figure A-5. Thus, the depth of modulation of the burst indicates the size of the particle which produced it.

The high-frequency Doppler and lower-frequency pedestal component amplitudes, DOP and PED, respectively, are defined as

$$DOP = \frac{I_{max} - I_{min}}{2} \tag{4}$$

$$PED = \frac{I_{max} + I_{min}}{2} \tag{5}$$

where I_{max} is the maximum signal amplitude and I_{min} is the next relative minimum signal amplitude as shown in Figures A-5 and A-6.

In optical work, the depth of modulation of the signal is called its visibility. This visibility, V, is defined as

$$V = \frac{PED}{DOP} = \frac{I_{max} - I_{min}}{I_{max} + I_{min}}. \tag{6}$$

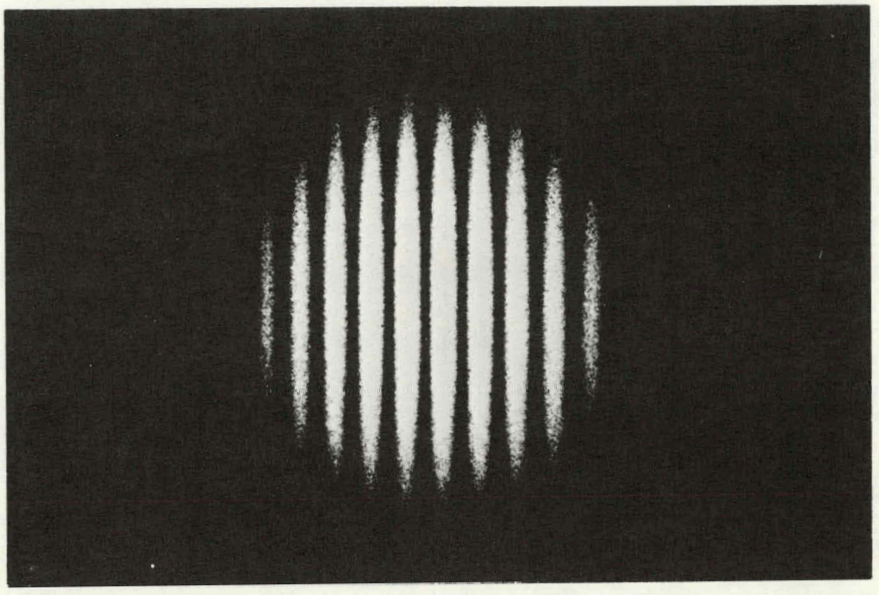

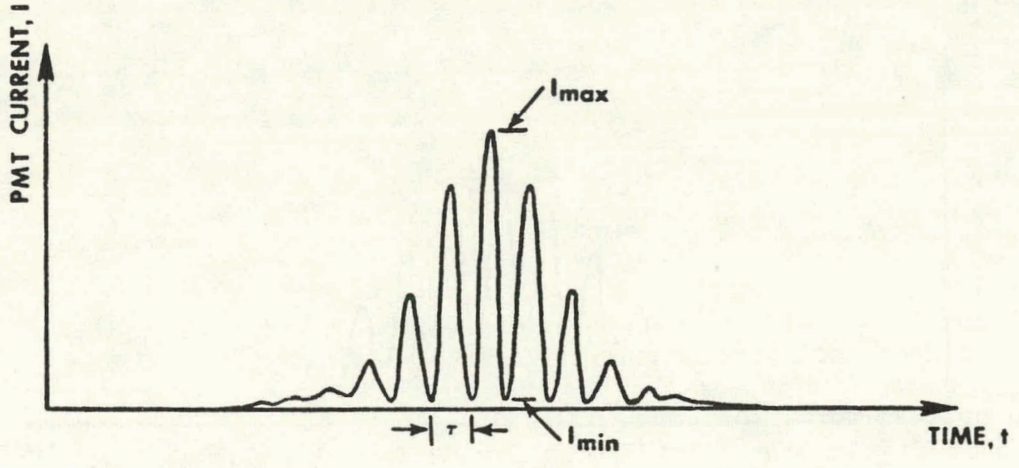

Figure A-5 PMT Signal Produced by a Particle With a Diameter Much Smaller Than δ

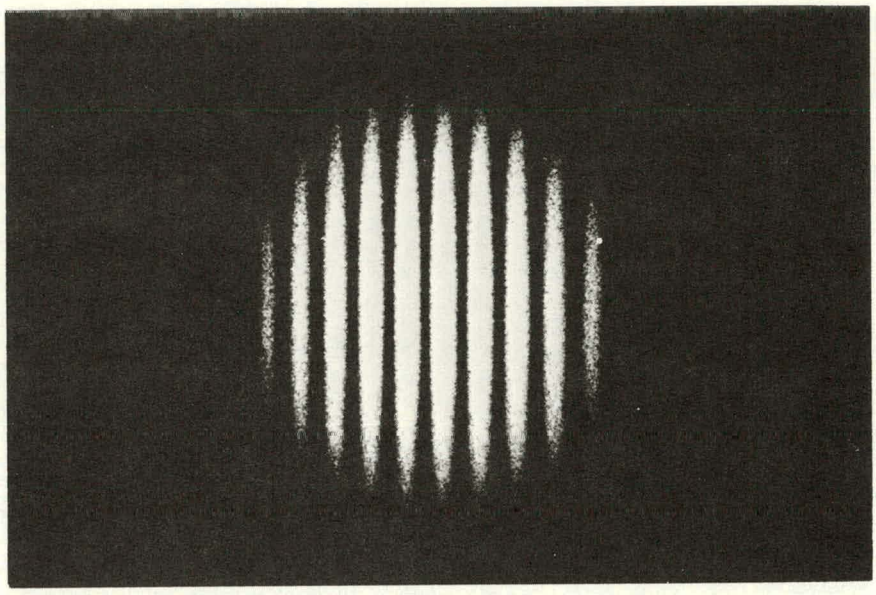

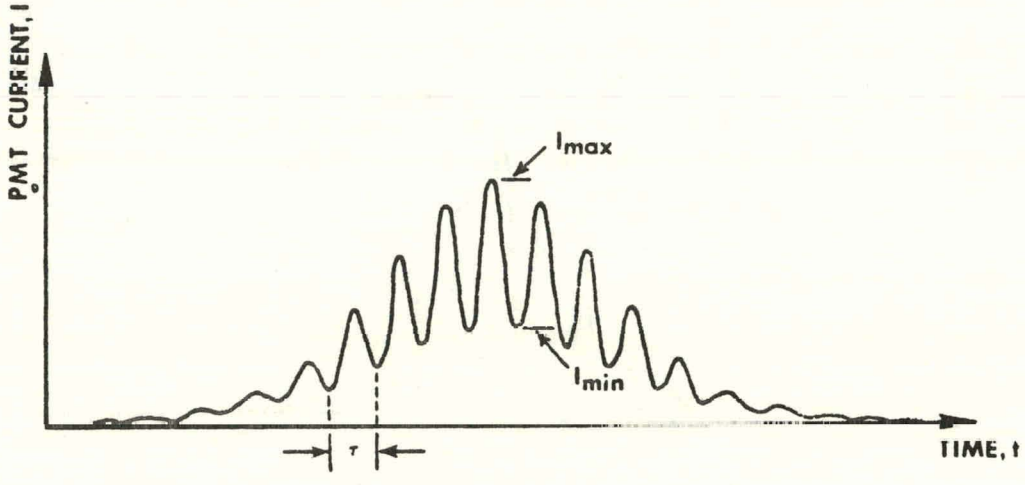

Figure A-6 PMT Signal Produced By a Particle With a Diameter of About δ/2

A particle much smaller than the fringe spacing will have a visibility near 1.0 since its I_{min} is nearly 0, but with larger particles where I_{min} approaches the value of I_{max}, the visibility will approach 0.

Through some rather complicated mathematical manipulations, it is possible to show that visibility can also be calculated from the ratio of two integrals. Let PED be the integral of the total signal and DOP be $\pi/2$ times the integral of the absolute value of the Doppler component, with both integrals being taken over the same integer number of fringe periods. Using these values for DOP and PED, it can be shown that the visibility is still given by Equation (6).

This fact can easily be verified by calculating the visibility of an artificial signal, shown in Figure A-7, which consists of 2 ma, peak-to-peak, since wave added to a 2 ma DC offset. Using the indicated values of I_{max} and I_{min}, Equation (6) gives the visibility of this signal to be 1/2. Integrating over one period of the signal, we get the following values for PED and DOP

$$PED = \int_0^{2\pi} [2 + \sin(x)]\, dx = 4\pi \tag{7}$$

and

$$DOP = \pi/2\ [\int_0^{\pi} \sin(x)\, dx + \int_{\pi}^{2\pi} -\sin(x)\, dx] = 2\pi . \tag{8}$$

Taking the ratio of these two integrals as shown in Equation (6) gives a visibility of 1/2, just as we previously calculated.

The relationship between particle sizes and their visibilities depends upon the shape of the particles. If we assume that they are spherical and that the PMT is focused on the probe volume along an axis bisecting the two laser beams, then visibility is related to the particle's mean diameter, D, by

$$v = \frac{2\ J1(\pi D/\delta)}{\pi D/\delta} \tag{9}$$

where δ is the fringe spacing and J1 is a first order Bessel function of the first kind. Similar relationships may be derived by assuming other particle shapes. Thus, in order to determine a particle's size, one needs a signal visibility analyzer (SVA) which will measure the DOP and PED values.

The block diagram in Figure A-8 illustrates the operation of a complete SVA. It is designed to be connected to and operated with an LV burst processor. The PMT output first passes through a preamp which buffers and amplifies the signal so that it can be transmitted down a 50 ohm coaxial cable to the SVA. In addition to the Doppler and pedestal components, this signal also contains a DC component caused by stray light striking the PMT.

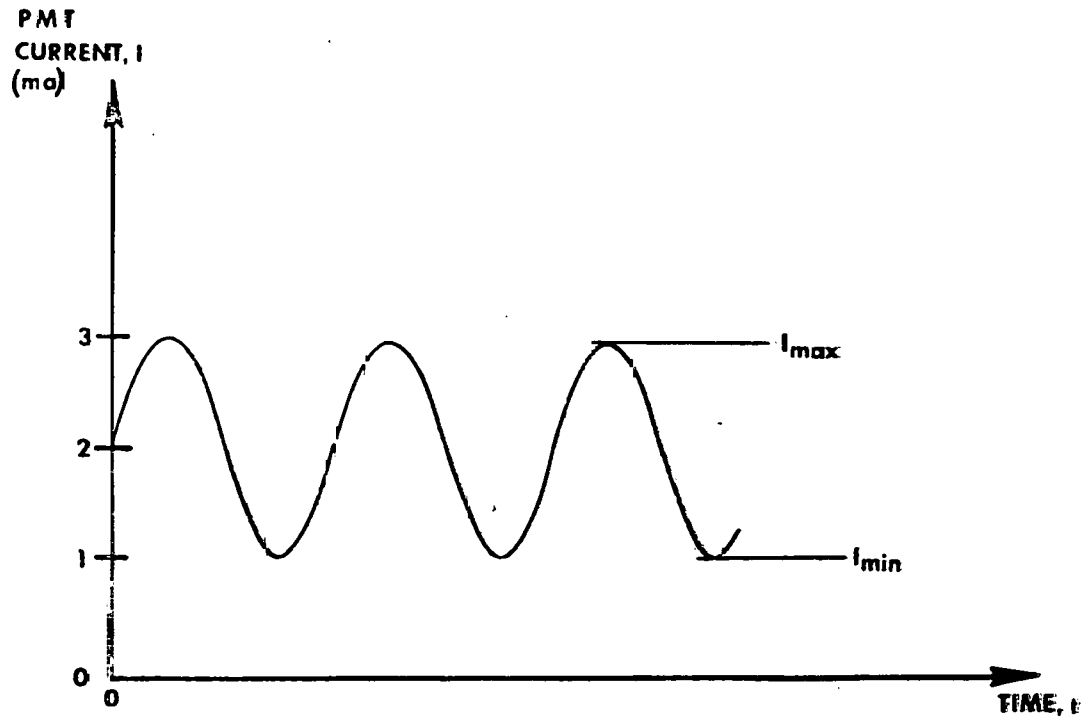

Figure A-7 Artificially Generated Signal With a Visibility of 1/2

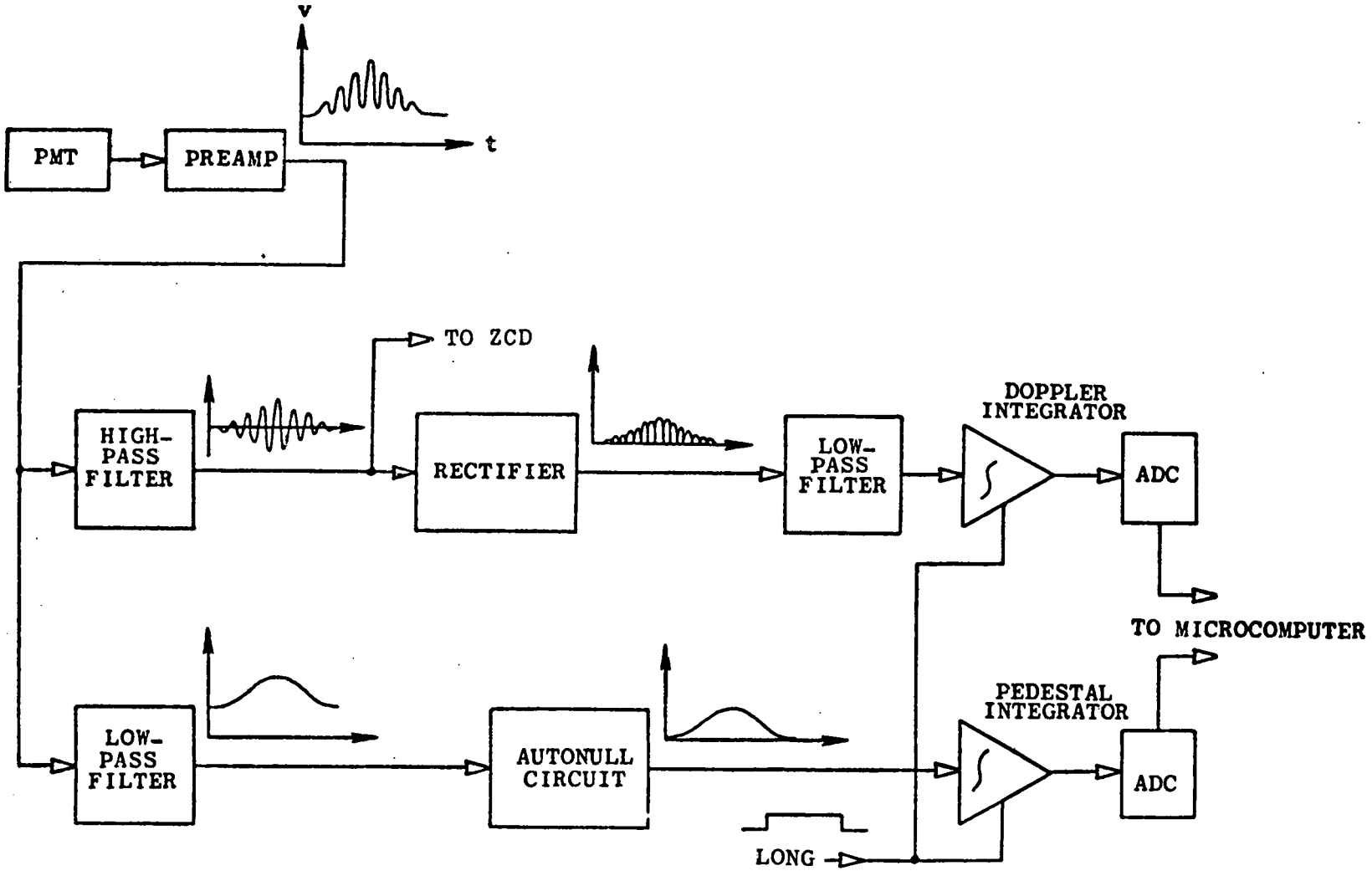

Figure A-8 Block Diagram of the Signal Visibility Analyzer

The higher frequency Doppler component is extracted through a high-pass filter having a cutoff frequency selected by the operator in accordance to the expected particle velocities. This signal serves as the ZCD input for the LV processor which measures its frequency. The amplitude of the Doppler component is measured by an AC integrating voltmeter, consisting of a rectifier, a low-pass filter, and an integrator. The rectifier is a precision circuit whose output is (theoretically, at least) the absolute value of its input. This unipolar output voltage is then integrated for the length of time, $N\tau$, that the LONG pulse from the LV processor is high.

A low-pass filter is used to extract the pedestal component of the burst. Accompanying this signal will be an extraneous DC voltage generated by effects such as PMT dark currents and unwanted light striking the PMT. Before the pedestal component can be properly measured, this DC offset must be removed by an autonull circuit which will be further described later. The pedestal voltage is then integrated simultaneously with the Doppler component.

At the completion of the integration time, the integrators' outputs are digitized by analog-to-digital converters (ADC's) and read by the microcomputer which later calculates the visibility from Equation (6) where DOP is now the output from the Doppler integrator and PED is the output from the pedestal integrator. Amplifier gains in the SVA are adjusted so that DOP = PED when a signal with a visibility of 1.0 is applied to the processor.

Before the pedestal signal is integrated, the extraneous DC level must be removed by the autonull circuit. However, this unwanted level shift must not be confused with the DC component of the actual signal burst. Therefore, the DC shift must be measured only when no signal bursts are present. This is accomplished in the autonull circuit by measuring the DC shift only while there is no ZCD pulse train present.

Figure A-9 is a block diagram which will help to explain the operation of the autonull circuit. The input signal (pedestal plus DC offset) first goes into a low-pass sample-and-hold (S&H) circuit. In the sample mode, this circuit acts like a 100 Hz low-pass filter which passes the DC voltage. The presence of a ZCD pulse train switches the S&H into its hold mode, and its output stays constant regardless of changes in the input voltage. The hold pulse is generated by a ZCD activity detector which consists of a retriggerable monostable multivibrator. Thus the S&H output is the DC offset voltage without the influence of the signal bursts.

In accordance with a microcomputer command, this DC voltage is digitized by an ADC. The ADC output is then read by the microcomputer which determines if the DC level is too high to allow proper measurements. If the voltage is too high, the instrument is reset and more measurement attempts are made until the DC drops to an acceptable level.

The ADC output also goes to a corresponding digital-to-analog converter (DAC) which reconstructs the original DC voltage. The ADC-DAC combination forms a sample-and-hold device with unlimited hold time. Subtracting the DAC output from the original input signal leaves the pedestal component without the DC offset. This is the signal which is then sent to the pedestal integrator.

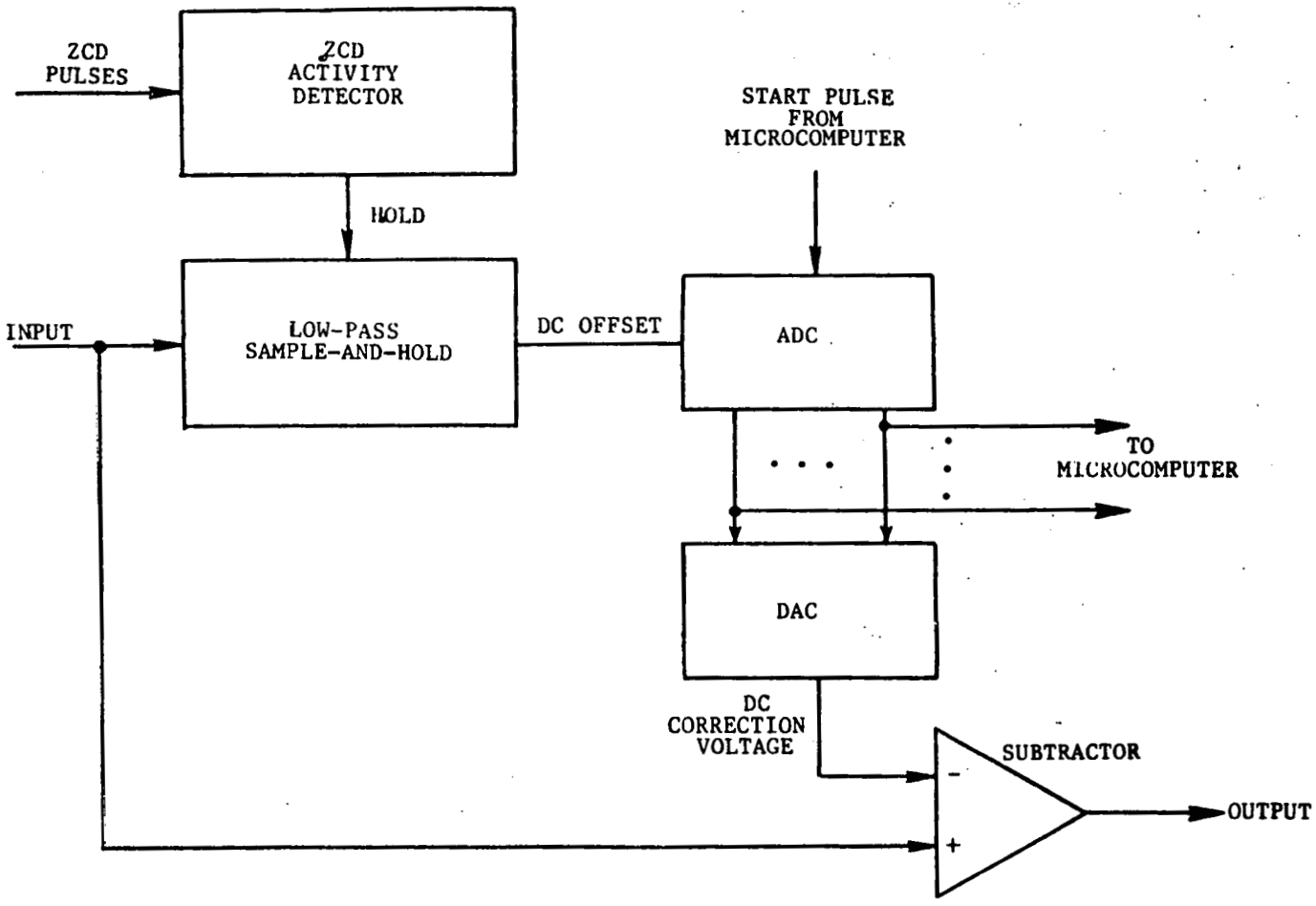

Figure A-9 Block Diagram of the Autonull Circuit

Further explanation should also be given to the integrators which are shown oversimplified in Figure A-8. Suppose that during normal operation the input voltage to an integrator varies over a range of 100 to 1, and the integration time (inversely proportional to the Doppler frequency) also varies over a range of 100 to 1. Thus, the output of the integrator will vary over a range of 10,000 to 1. It is impractical to build any electronic integrator which will operate linearly over such a wide dynamic range, and the ADC would not give adequate resolution on the lower output voltages.

To overcome these problems, each integrator is actually constructed out of four integrators in an autoranging arrangement as shown in Figure A-10. Each of these latter integrator outputs covers a range of 1 to 10; thus, the four cover a range of four decades. Their integration time constants are in consecutive orders of 10, i.e. when the output of the most sensitive integrator is 10 volts, the other outputs will be 1 volt, 0.1 volt, and 0.01 volt, with the last being the least sensitive integrator. An analog multiplexer selects one integrator output, starting with the most sensitive, and sends it to the ADC. This output is compared to a reference voltage of 10 volts, and whenever it exceeds that value, the next lower integrator output is selected. Two range bits indicate to the microcomputer by what power of ten to multiply the ADC output. Therefore, four decades of integration are covered while the ADC input remains between 1 and 10 volts, allowing good resolution.

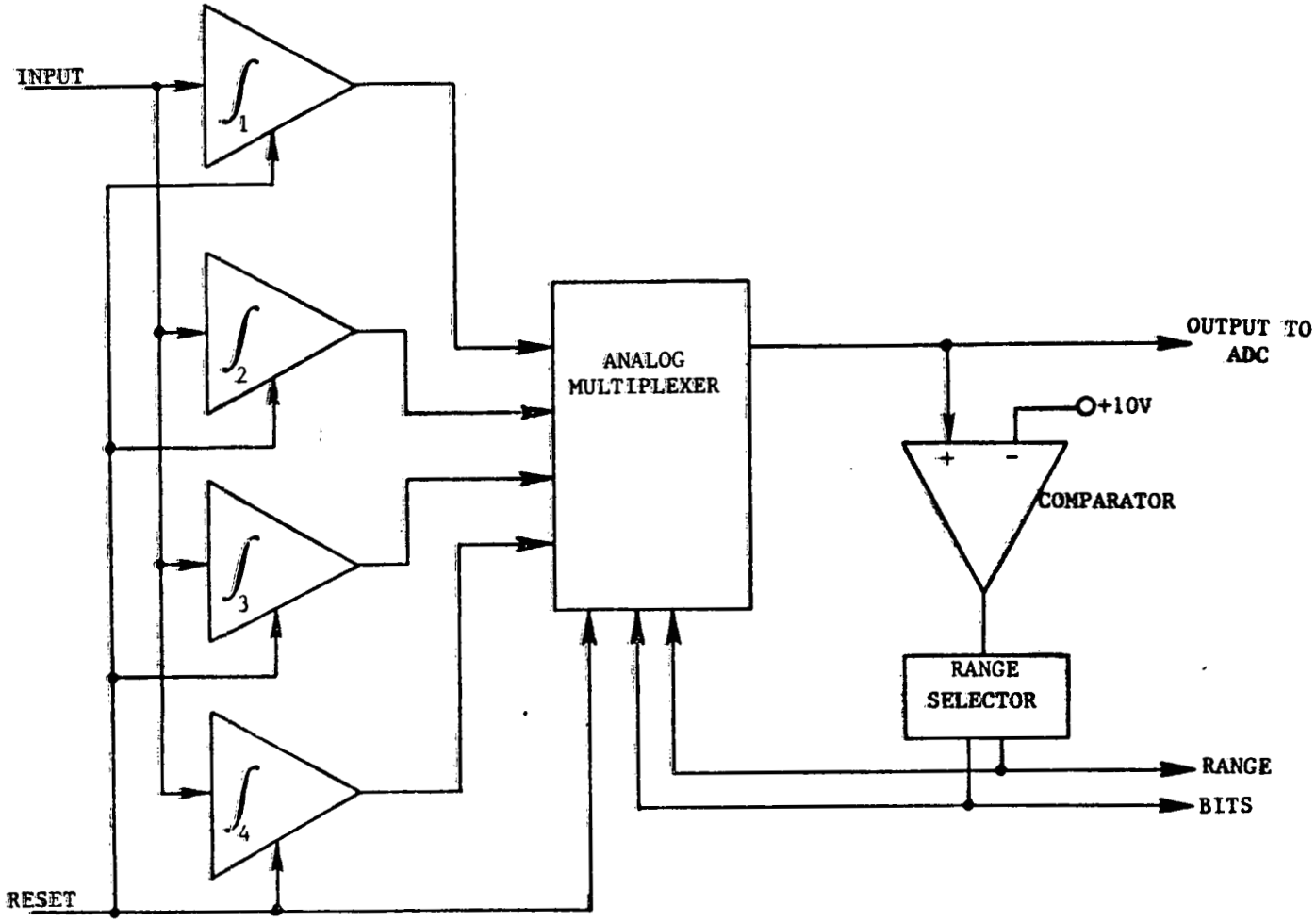

Figure A-10 Block Diagram of the Autoranging Integrators

U.S. GOVERNMENT PRINTING OFFICE 1984—746-081/2559